One-year Continuous Observations of Near-Surface Atmospheric Water Vapor Stable Isotopes at Matara, Sri Lanka

Yuqing Wu [1, 2], Jing Gao [1, 3, *], Aibin Zhao [1], Xiaowei Niu [1], Yigang Liu [1, 2], Disna Ratnasekera [4, 5], Tilak Priyadarshana Gamage [6], Amarasinghe Hewage Ruwan Samantha [6]

1 State Key Laboratory of Tibetan Plateau Earth System, Resources and Environment, Institute of Tibetan Plateau Research, Chinese Academy of Sciences, Beijing 100101, China

2 University of the Chinese Academy of Sciences, Beijing, 100049, China

3 Lanzhou University, Lanzhou 733000, China

4 China-Sri Lanka Joint Center for Education & Research, Guangzhou 510301, China

5 Department of Agricultural Biology, Faculty of Agriculture, University of Ruhuna, Matara 81000, Sri Lanka

6 Faculty of Fisheries and Marine Sciences & Technology, University of Ruhuna, Matara 81000, Sri Lanka

* *Corresponding author*: Jing Gao (gaojing@itpcas.ac.cn)

Abstract:

Atmospheric water vapor stable isotopes are crucial for understanding hydrological cycle processes under climate change. This study presents the results from a year-long in-situ monitoring of atmospheric water vapor stable isotopes ($\delta^{18}O$, δD) at Matara, Sri Lanka, from March 2020 to February 2021 to assess how oceanic sources and moisture transport influence coastal atmospheric moisture isotopic composition. We identified clear seasonal patterns in the isotopic composition, with $\delta^{18}O$, δD, and d-excess showing substantial variation between the southwest and northeast monsoon periods. The primary moisture sources were the Arabian Sea and the Indian Ocean during the southwest monsoon (May to September), characterized by lower amplitude values of $\delta^{18}O$ (-20.4‰ to -9.1‰). During the northeast monsoon, the northern Bay of

Bengal, the Indian subcontinent, and Southeast Asia were primary moisture sources, resulting higher amplitude values of $\delta^{18}O$ (-23.9‰ to -7.5‰) and higher d-excess values (up to 25 ‰). The study also identified significant influences of sea surface temperature and sea surface relative humidity on the isotopic composition of water vapor. Additionally, we could use outgoing longwave radiation (OLR) to gauge the intensity of convective activity. Lower OLR values, indicative of stronger and deeper convection, were associated with air masses that were more depleted in $\delta^{18}O$. These findings facilitate a better understanding of how the monsoon and local meteorological conditions affect water vapor isotope compositions in tropical region. Furthermore, we present a new dataset that should enable improved water vapor isotopic modeling and projections of atmospheric processes in coastal regions.

Keywords: Indian Summer Monsoon, Water Vapor Isotopes, Sea Surface Condition, Convective Activity, Sri Lanka

Short Summary

Monitoring of atmospheric water vapor isotopes for one year at Matara, Sri Lanka, yielded clear seasonal variations in $\delta^{18}O$, δD, and d-excess. The results showed lower amplitudes of $\delta^{18}O$ during the southwest monsoon and higher amplitudes of $\delta^{18}O$ and higher d-excess during the northeast monsoon. Sea surface evaporation and regional convective activity significantly influenced isotopic compositions. Overall, our results facilitate an improved understanding of the impacts of monsoon and local meteorological conditions on tropical water vapor isotopic composition.

1 Introduction

The Indian Summer Monsoon (ISM), occurring from June to September, is a pivotal component of the Asian climate system, serving as the primary transport of moisture from the Indian Ocean to the Indian subcontinent and the Tibetan Plateau (TP). Monsoonal precipitation plays a crucial role in agriculture and water resource avaliability, affecting the welfare of over 1.9 billion people in surrounding countries

(Webster et al., 1998; Goswami et al., 2016). The Tibetan climate and hydrology are profoundly influenced by the ISM, as it contributes significantly to the regional water cycle by delivering substantial rainfall during the summer months. This rainfall is essential for maintaining the glaciers and permafrost in the TP, a key water catchment area for many of Asia's largest rivers (Bookhagen and Burbank, 2010). The ISM's intensity and variability can lead to significant fluctuations in water availability, affecting both agriculture and hydropower generation in the region (Singh and Bengtsson, 2004; Gao et al., 2014). Furthermore, the interaction between the ISM and the TP's topography creates unique climatic conditions that influence weather patterns and extreme events in the region (Liu and Chen, 2000).

The seasonal precipitation and its origins over the TP are inextricably linked to the dynamics of the ISM (Dai et al., 2021). Previous studies have provided evidence that isotopic records derived from precipitation over the TP offer insights into the climatic fluctuations and distinct moisture attributes associated with the ISM (Gao et al., 2013; Guo et al., 2017). The summer monsoon brings significant moisture from the Indian Ocean, leading to substantial rainfall over the TP primarily during the monsoon months of June-September (Yao et al., 2012). This seasonal influx of moisture is critical for maintaining the regional hydrological balance and supporting ecosystems. Furthermore, the ISM’ s intensity and variability significantly influence the interannual and decadal precipitation patterns over the TP, affecting the overall water availability and climatic stability of the region (Kaushal et al., 2018).

The stable isotopic composition of river water (Bershaw et al., 2012; Li and Garzione, 2017), precipitation (Rahul et al., 2016a; Cai et al., 2017), and water vapor (Risi et al., 2008; Steen-Larsen et al., 2013b; Rahul et al., 2016b; Lekshmy et al., 2022) serves as a valuable tool for identifying the origins and understanding transmission processes of atmospheric water vapor. Fractionation occurs during various phase transitions, such as sea surface evaporation, condensation beneath clouds, re-evaporation of raindrops, and diffusive exchanges between water vapor and raindrops (Stewart, 1975; Benetti et al., 2018; Graf et al., 2019). The occurrence of fractionation unveils investigable spatiotemporal distribution patterns in the water isotopic composition, encompassing water vapor and precipitation. In this context, deuterium excess (d-excess = $\delta D - 8 \times \delta^{18}O$) is a useful parameter for studying kinetic fractionation effects (Dansgaard, 1964). Recent studies have significantly enhanced our understanding of isotopic signals in convection regions, elucidating the complex interactions between moisture processes and isotopic composition in tropical deep convection. Around Barbados, during the winter trade winds, vertical transport and large-scale circulation have been identified as primary drivers of isotopic variability at the cloud base, acting over timescales from hours to days (Bailey et al., 2023; Villiger and Aemisegger, 2024). Investigations into water vapor isotopes in the West African troposphere reveal that both convection and mixing highlight the important role played by large-scale atmospheric circulation processes in the variations of water vapor isotopes (Diekmann et al., 2021; de Vries et al., 2022). The precise mechanisms by which convective activity reduces the amount of stable isotopes in water vapor and precipitation are still under debate. Some researchers have emphasized the significance of condensation levels (Cai and Tian, 2016; Permana et al., 2016; Thompson et al., 2017), while others suggested raindrop re-evaporation and raindrop-vapor isotope exchanges during strong convection as crucial factors (Galewsky et al., 2016). Additionally, unsaturated or mesoscale descending airflows that transport vapor depleted in heavy isotopes to the lower atmosphere also contribute to lower isotope values (Risi et al., 2008; Kurita, 2013). The influence of these processes varies with the intensity of convective activity.

Evaporation at the ocean surface constitutes a significant component of the global water cycle and is pivotal for the accurate modeling of climate change. Typically, research on water vapor stable isotopes in the marine boundary layer aims to elucidate the processes associated with evaporation isotopes as well as influencing factors (Craig and Gordon, 1965). The d-excess of evaporated water vapor is mainly impacted by dynamic fractionation associated with sea surface temperature (SST), the relative humidity above the sea-surface (RH_{SST}, calculated relative to the saturation vapor pressure at SST), and wind speed (rough or smooth) (Benetti et al., 2015; Benetti et al., 2018). Investigations into the water vapor stable isotopic composition within the marine boundary layer have been principally focused on regions such as the North Atlantic (e.g., Greenland, Iceland, Bermuda) (Steen-Larsen et al., 2013a; Bonne et al., 2014; Benetti et al., 2018; Bonne et al., 2019), Bay of Bengal (BoB) (Lekshmy et al., 2022), and Arctic Oceans (Kurita, 2011). Several studies could confirm the existence of a negative relationship between d-excess and RH_{SST} (Uemura et al., 2008; Steen-Larsen et al., 2015), with wind speed and SST exerting a limited influence on this correlation (Benetti et al., 2015). Observations from the North Atlantic support this theory (Benetti et al., 2014). In addition, studies found significant variations in d-excess values in vapor that originated at different moisture sources (Kurita, 2011; Steen-Larsen et al., 2013b; Delattre et al., 2015). Subsequently, Benetti et al. (2015) introduced a multi-layer mixing model, which is expected to improve the accuracy of d-excess and water vapor isotope simulations. Due to the impact of dynamic fractionation on sea surface water evaporation, some studies have focused on simulating observed d-excess under the closure assumption (Bonne et al., 2019). Others have used isotope atmospheric circulation models to assess mixing and transport processes within the marine boundary layer (Benetti et al., 2015). Owing to the minor influence of transport-induced fractionation, d-excess in the marine boundary layer is typically employed to deduce moisture sources (Benetti et al., 2018).

Amidst the backdrop of global climate change, observing stable isotopes in atmospheric water vapor is vital for monitoring and understanding climate shifts in low-latitude areas (Rahul et al., 2016b). Such research is instrumental for providing a deeper understanding of near-surface water vapor dynamics, pinpointing vapor sources and transport routes, and differentiating between different contributions of atmospheric water vapor to the water cycle.

Located in the northern Indian Ocean, Sri Lanka is impacted by both the southwest and northeast monsoons (Fig. 1a, b) and has been identified as an important origin region for monsoonal water vapor over the TP. However, only few studies have focused on the Indian Ocean, and even fewer on the area around Sri Lanka. This knowledge gap underscores the need to explore isotopic signals in this region and place them into their appropriate context, e.g., with findings by Risi et al. (2008). For instance, more recent studies on water stable isotopes in the South Indian Ocean and South Asian region have uncovered connections between local processes and large-scale atmospheric circulation, shedding light on sea-surface dynamics (Midhun et al., 2013; Rahul et al., 2016b; Bonne et al., 2019). Unlike, in precipitation and surface water, in atmospheric water vapor stable isotopes can be monitored continuously regardless of season, weather, or location (Angert et al., 2008). This potentially full temporal and spatial coverage allows for a more comprehensive and continuous monitoring of atmospheric water vapor dynamics and transport, which should in turn facilitate a deeper understanding of isotope transformation processes within the water cycle. Therefore, investigating the dynamics of near-surface atmospheric water vapor stable isotopes at coastal stations is not only pivotal for identifying monsoonal water vapor source regions but will facilitate a better understanding of precipitation processes over the Indian Ocean. Oceanic evaporation represents the first of many phase transitions that occur during the global water cycle. The primary objective of researching water vapor stable isotopes is to comprehend the processes and controlling factors of water isotopic variations.

In this study, we present the results from continuous observations of near-surface atmospheric water vapor stable isotopes in Matara, Sri Lanka, collected from March 1, 2020, to February 28, 2021. We analyze the observational data to gain a better understanding of the variations in moisture sources and main transmission processes in tropical coastal regions. Furthermore, we explore how sea surface processes, convective activity, and local meteorological factors affect near-surface atmospheric water vapor stable isotopes at a coastal station, across daily, monthly, and seasonal (monsoonal) time scales. Section 2 gives an overview of the study site and presents the meteorological and water vapor observations, calibration protocols, and analysis methods. In Section 3, we illustrate the variability of isotopic and meteorological parameters, analyze moisture sources, assess the impact of sea surface processes on water vapor isotopes, and explore the relationship between water vapor isotopes, convective activity, and local meteorological observations.

2 Study Site, Data, and Methods

2.1 Study Site and Meteorological Data

Sri Lanka (located between approximately 6°N to 10°N and 79° to 82°E) is the southernmost country on the Indian subcontinent and a key region for identifying the moisture source of the south Asian summer monsoon (Ravisankar et al., 2015). Featuring a tropical climate, Sri Lanka experiences four distinct monsoon seasons annually: the northeast monsoon from December to February, the first inter-monsoon from March to April, the southwest monsoon from May to September, and the second inter-monsoon from October to November (Malmgren et al., 2003; Jayasena et al., 2008). For the analyses, we combined the first and second inter-monsoon periods into a single “non-monsoon period”. Most of the precipitation in Sri Lanka comes from the southwest and northeast monsoon systems, accounting for over 78% of the total annual precipitation (Fig. 1c). Precipitation formation in Sri Lanka primarily relies on organized convection associated with the Intertropical Convergence Zone (ITCZ) and low-pressure systems (Gadgil, 2003), while the associated moisture primarily originate in the Indian Ocean and BoB (Bandara et al., 2022). The southwest monsoon transports moisture from the Indian Ocean to southwestern Sri Lanka (Fig. 1a) where it leads to increased rainfall (Bavadekar and Mooley, 1981). In contrast, the northeast monsoon carries water vapor from the BoB to northern and northeastern of Sri Lanka (Fig. 1b) (Dhar and Rakhecha, 1983; Wang, 2006).

An automated weather station (AWS) was installed at the University of Ruhuna, Matara (located at 5.94°N, 80.57°E) on the southern coast of Sri Lanka (Fig. 1d). It collected real-time meteorological observations, including air temperature, precipitation, relative humidity, air pressure, wind speed, and wind direction, from March 1, 2020, to February 28, 2021. Based on the measured air temperature, relative humidity, and air pressure, we can compute the lifting condensation level (LCL) using

(Dirmeyer et al., 2013):

$$\log E = -7.90298 \times (\frac{373.16}{T_{\text{obs. air}}} - 1) + 5.02808 \times \log 10(\frac{373.16}{T_{\text{obs. air}}}) -$$

$$1.3816 \times 10^{-7} \times (10^{(11.344 \times (1 - \frac{T_{\text{obs. air}}}{373.16})) - 1)} + \tag{1}$$

$$8.1328 \times 10^{-3} \times (10^{(-3.49149 \times (\frac{373.16}{T_{\text{obs. air}}} - 1)}) - 1) + \log 10(1013.246)$$

$$E_{\text{true}} = E \times RH \tag{2}$$

$$W = 0.622 \times \frac{E_{\text{true}}}{P - E_{\text{true}}} \tag{3}$$

$$T_{\text{dew}} = \frac{B}{\log\left(\frac{A \times 0.622}{W \times P}\right)} \tag{4}$$

$$LCL = 125 \times (T_{\text{obs. air}} - T_{\text{dew}}) \tag{5}$$

where E is the saturated vapor pressure, obtained from the improved Goff-Gratch formula (Goff and Gratch, 1946); E_{true} is the actual water vapor pressure; RH and W are relative humidity and mixing ratio, respectively; $T_{\text{obs. air}}$ and T_{dew} are the air temperature measured directly by the AWS and dew point temperature, respectively; P is the air pressure. The constants A and B have values of 2.53×10^8 kPa and 5.42×10^3, respectively.

Meteorological data are compared with water vapor isotopic data measured during the same period. Based on the European Centre for Medium-Range Weather Forecasts (ECMWF, https://cds.climate.copernicus.eu/eu/) reanalysis dataset (ERA5), the annual average precipitation and air temperature for the period from 2000 to 2020 is 2085 mm and 27.6 °C, respectively (Fig. 1c) (Hersbach et al., 2020).

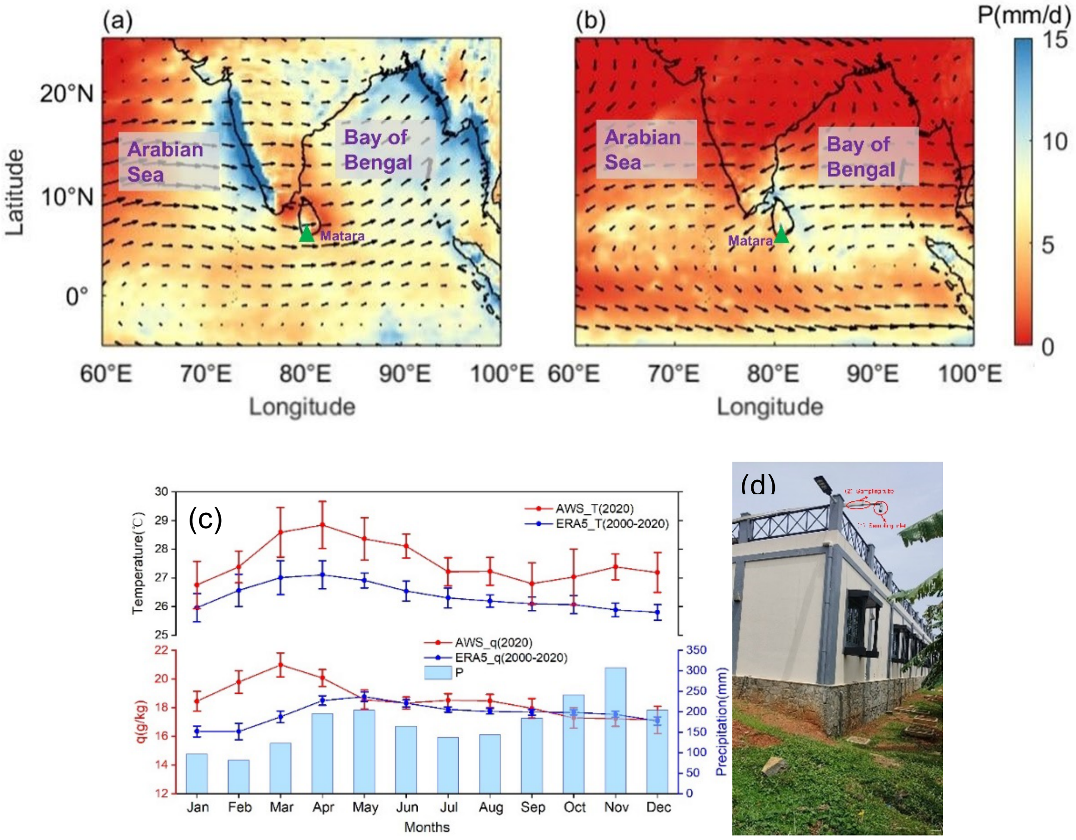

Figure 1: Mean wind vectors (arrows) at 850 hPa during the (a) 2020 southwest monsoon and (b) 2020/2021 northeast monsoon seasons, along with mean precipitation (P, base colors) from ERA5 averaged for the same period. (c) Monthly mean temperature and specific humidity (q) obtained from the automated weather station at Matara (January and February are from 2021 while March – December from 2020), with monthly average temperature, specific humidity, and precipitation from ERA5 (averaged for the years 2000-2020) plotted for comparison. (d) Photograph of the roof-mounted weather station at the University of Ruhuna, Sri Lanka.

In this study, we used daily and monthly averages of outgoing longwave radiation (OLR, https://www.esrl.noaa.gov/psd/data/gridded/data.ncep.reanalysis.pressure.html) to quantify the convective activity. In addition, we used hourly data of 2m air temperature, 2m dew temperature, air pressure, precipitation, SST, atmospheric boundary layer height (BLH), wind speed, and wind direction, obtained from ERA5 for years 2000 to 2021, with a spatial resolution of 0.25°×0.25° and a temporal resolution of one hour. Studies have shown that ERA5 data provide good representations of the Matara equatorial climate and can be used in lieu of missing observational data

(Bandara et al., 2022). Due to weather conditions and instrument trouble, specific humidity measured by the isotopic measurement instrument and computed by the AWS are missing from March, 2020 to April, 2020. Therefore, we chose to present both variables obtained from ERA5 as they complement each other, providing a clearer picture of humidity changes at Matara station.

For the atmosphere above open sea regions, RH_{SST} is obtained using (Bonne et al., 2019):

$$RH_{SST} = RH_{2m\ air} \times \frac{q_{sat}(T_{2m\ air})}{q_{sat}(SST)} \tag{6}$$

where $RH_{2m\ air}$ is the relative humidity 2m above the ocean surface, $q_{sat}(T_{2m\ air})$ is the specific humidity at a saturated condition for a given 2m air temperature, and $q_{sat}(SST)$ is calculated for seawater with a salinity of 35 practical salinity units (PSU) (Curry and Webster, 1999).

The formulas to calculate air saturation specific humidity $q_{sat}(T_{air})$ and sea surface saturation specific humidity $q_{sat}(SST)$ (sea surface salinity of 35 PSU) are:

$$q_{sat}(T_{air}) = \frac{0.622 \times E}{P} \tag{7}$$

$$q_{sat}(SST)\text{ (sea surface salinity of 35 PSU)} = 0.98 \times q_s\text{(sea surface salinity of 35 PSU)} \tag{8}$$

q_s(sea surface salinity of 35 PSU) represents specific humidity and is calculated in the same way as $q_{sat}(T_{air})$. E is the saturated water vapor pressure, obtained from the improved Goff-Gratch formula (Goff and Gratch, 1946) and P is atmospheric pressure. Sea surface pressure is calculated using atmospheric pressure.

2.2 In-situ Observations of Atmospheric Water Vapor Isotopic Composition

Near-surface atmospheric water vapor isotope measurements at Matara were collected using a sampling frequency of 1Hz with the instrument located approximately

5m from the AWS. We used a Water Vapor Isotope Analyzer (Los Gatos Research (LGR) Inc.) in conjunction with an LGR Water Vapor Isotope Standard Source (WVISS) model. The LGR instrument employs a mirrored sampling chamber in which the laser traverses the sample volume thousands of times, effectively amplifying the water vapor absorption signal which facilitates the detection of low concentrations of D and ^{18}O (Liu et al., 2015). Compared to traditional methods, this spectroscopic technique offers three advantages: (i) it is compact and portable, enabling real-time field monitoring; (ii) it can simultaneously measure δ^{18}O and δD; and (iii) it has lower measurement costs and requires less operator expertise.

The instrumental setup was situated approximately 100 m from the sea shore (5.94° N, 80.57° E, 10 meters), and consisted of four primary components: (1) A sampling inlet, positioned approximately 5 m above the ground (Fig. 1d), equipped with a stainless-steel mesh to prevent interference from insects and facing downward to avoid direct impacts from rain. (2) A 1/4-inch outer diameter stainless steel sampling tube, insulated with heating tape and a 2-cm thick pipe for thermal insulation. (3) The calibration unit to generate a constant flow of water vapor with known isotopic composition and at different humidity levels. (4) A water vapor isotope analyzer, delivering a measurement precision for δ^{18}O and δD of 0.25‰ and 0.5‰, respectively (a concentration of 2500 ppmv). This setup has been designed to minimize external influences and maintain the integrity of the sampled water vapor.

The spatial proximity between the water vapor analyzer and AWS ensures a high level of synchronicity between the isotope and meteorological measurements. We define wind directions from 60° to 330°N as oceanic, while those from 330° to 60°N as terrestrial winds (Fig. 1a, b).

Atmospheric water vapor stable isotopes are expressed using the δ notation (in per mil, ‰), using the following equations:

$$R_{^{18}O} = \frac{^{18}O}{^{16}O} \tag{9}$$

$$R_D = \frac{D}{^{1}H} \tag{10}$$

$$\delta_{\mathrm{sample}} = \left(\frac{R_{\mathrm{sample}}}{R_{\mathrm{VSMOW}}} - 1\right) \times 1000‰ \tag{11}$$

Here, δ_{sample} represents either $\delta^{18}O$ or δD (^{18}O or D isotope ratio) relative to Vienna Standard Mean Ocean Water (VSMOW). R_{sample} and R_{VSMOW} are the ^{18}O or D and VSMOW isotope ratios, respectively.

2.3 Calibration Protocol

In this study, we adhere to the calibration protocol proposed by Steen-Larsen et al. (2013b). Briefly, the instrument calibration and data processing consist of three major steps: (1) humidity-isotope response calibration, (2) VSMOW - Standard Light Antarctic Precipitation (VSMOW-SLAP) calibration, and (3) drift correction (see Text S1 in the Supporting Information).

The water vapor concentration can influence the measured water vapor isotopic composition, known as concentration- or humidity-isotope dependency characterization. By adding a constant stream of water vapor with known isotopic composition at different humidity levels, we can establish the humidity-isotope response function (Sturm and Knohl, 2010; Aemisegger et al., 2012). As this function can vary over time, its calibration was repeated monthly, using two standard samples of known isotopic compositions measured at humidity levels ranging from 16,000 to 38,000 ppmv at intervals of 1000 ppmv. Each level was measured for at least 25 minutes using the LGR WVISS. Our results are referenced to a humidity level of 20,000 ppmv. We compared our measurements to the international VSMOW-SLAP scale, assuming a linear drift between calibration points.

To compensate for instrumental drift, we measured the water vapor from a drift-standard bottle for 25 minutes after each 12 hours performed an ambient air measurement. Furthermore, we tested for instrument drift as part of the routine instrument maintenance, assuming a linear drift between each drift-standard measurement. Laboratory analyses of liquid isotopes have confirmed the stability of its isotopic composition over time.

2.4 Rayleigh Distillation Model and MBL-Mixing Model

The Rayleigh distillation model is employed to quantify isotopic variations during phase changes (Dansgaard, 1964), by which the residual air mass becomes drier with a depletion in heavy isotopes following moist adiabatic vertical ascent (Gat, 1996):

$$R_r = R_0 f^{\alpha_v^l(T) - 1} \tag{12}$$

Here, R_r and R_0 represent the isotopic ratio of residual vapor and initial vapor, respectively. $\alpha_v^l(T)$ denotes the equilibrium fractionation factor, and f is the fraction of residual water vapor.

By integrating the definition of isotope ratios as given in Equation (11), the Rayleigh distillation model can be expressed in terms of isotopic content as follows:

$$\delta_r = (\delta_0 + 1) f^{\alpha_v^l(T) - 1} - 1 \tag{13}$$

where δ_r and δ_0 are the isotope ratios relative to VSMOW in residual and initial vapor, respectively.

We employ the mixing model to examine the isotopic characteristics after the mixing of two air masses (Galewsky and Hurley, 2010):

$$R_{mix} = \frac{f[HDO]_1 + (1 - f) \times [HDO]_2}{f[H_2O]_1 + (1 - f) \times [H_2O]_2} \tag{14}$$

$$R_{mix} = \frac{f\left[H_2{}^{18}O\right]_1 + (1 - f) \times \left[H_2{}^{18}O\right]_2}{f[H_2O]_1 + (1 - f) \times [H_2O]_2} \tag{15}$$

where R_{mix} represents the isotopic ratio of the mixed air mass, while [HDO], $[H_2O]$, and $\left[H_2{}^{18}O\right]$ denote isotopic water vapor volume mixing ratios, and f is the mixing fraction.

We use water vapor isotopes to characterize the mixing processes in the marine boundary layer (MBL) (Benetti et al., 2018), using the following equation (Craig and Gordon, 1965):

$$1 + \delta_e = \frac{1}{\alpha_k} \times \frac{\alpha_v^l \times (1 + \delta_{OC}) - RH_{SST} \times (1 + \delta_{MBL})}{1 - RH_{SST}} \tag{16}$$

where α_v^l represents the equilibrium fractionation factor between vapor and liquid, and α_k is the kinetic fractionation factor. δ_{OC} denotes the isotopic composition of the ocean surface. We utilize α_v^l from Majoube (1971a, b) and α_k for the smooth regime ($\alpha_k{}^{18}O$ =

1.006 and $\alpha_k D = 1.0053$) (Merlivat and Jouzel, 1979).

2.5 Concentration-Weighted Trajectory and Moisture Source Diagnoses

To delineate water vapor transport paths and pinpoint moisture sources, we employed the Hybrid Single-Particle Lagrangian Integrated Trajectory (HYSPLIT) model from the US National Oceanic and Atmospheric Administration (NOAA) to compute backward trajectories of air masses arriving at Matara station during the southwest and northeast monsoons. The Global Data Assimilation System (GDAS) with 1°×1° and 3-hour spatial and temporal resolutions provided the background meteorological data from May 2020 to September 2020 and December 2020 to February 2021 (ftp://arlftp.arlhq.noaa.gov/archives/gdas1/). The HYSPLIT model uses GDAS reanalysis data, which contains 37 (vertical) pressure levels and a 1°×1° horizontal resolution. This enables the model to generate hourly outputs consisting of particle properties, locations, and relevant meteorological variables such as pressure, temperature, precipitation, and specific humidity. As atmospheric water vapor primarily resides at altitudes below 2 km (Wallace and Hobbs, 2006), we initiated the backward trajectories from a height of 50 m above the ground. Particles were released four times daily (at 00:00, 06:00, 12:00, and 18:00 UTC) at 20 different locations within a rectangular area extending 0.2° in each direction (north, south, east, and west) from Matara station and at four heights above the ground (50 m, 500 m, 1200 m, and 2000 m). Each trajectory was back-traced for 168 h, recording data at 1-h intervals. The HYSPLIT model outputs latitude, longitude, elevation, pressure, temperature, precipitation, relative humidity, and specific humidity. Backward trajectory clustering analysis was conducted, using the corresponding meteorological data. We averaged the trajectories of four times per day to obtain a daily mean trajectory, combined with water vapor stable isotope values on precipitation days. These daily mean trajectories were clustered by moisture source using K-means clustering. By analyzing the variations in latitude, elevation, and specific humidity along the trajectories, the influence of different moisture sources on local vapor content and isotopic composition was evaluated.

These analyses yielded concentration-weighted trajectory (CWT) fields (resolution of 0.5°×0.5°) (Hsu et al., 2003) using the in-situ daily average $\delta^{18}O$ and d-excess, which in turn facilitated the identification of potential moisture sources and an assessment of the potential influence of recirculation on d-excess in water vapor (Salamalikis et al., 2015; Bedaso and Wu, 2020; Xu et al., 2022). CWT (C_{ij}) was calculated as:

$$C_{ij} = \frac{\sum_{k=1}^{K} C_k \tau_{ijk}}{\sum_{k=1}^{K} \tau_{ijk}} \qquad (17)$$

where (i, j) denote grid coordinates, k the trajectory index, K the total number of trajectories analyzed, C_K the concentration (here $\delta^{18}O$ and d-excess) at the end of the trajectory k, and τ_{ijk} the residence time of trajectory k in grid cell (i, j). We substituted the residence time by the number of trajectory endpoints in each grid cell (i, j).

3 Results

3.1 Seasonal Variability of Water Vapor Stable Isotope

Fig. 2 shows the hourly and daily averages of water vapor isotopes ($\delta^{18}O$, δD, and d-excess) alongside temperature, relative humidity, atmospheric pressure, specific humidity, and SST at Matara station.

The mean relative humidity, specific humidity, lifting condensation level (LCL), monthly precipitation, and water vapor isotopic composition ($\delta^{18}O$, δD, and d-excess) exhibit a clear seasonal cycle (Fig. S3 and Table 1). The 12-month average temperature and relative humidity are 27.6°C and 80.7%, respectively (Table 1). Temperature variations maintain consistent amplitudes between monsoon and non-monsoon periods at around 10°C. Recorded minimum and maximum temperatures are 22.3°C and 33.5°C, respectively. Specifically, comparing monthly variations in air temperature and specific humidity (Fig. S3), both parameters gradually decrease from relatively high values in May to their respective minima of 26.9℃ and 18.5 g/kg (monthly averages) in September. Monthly average air temperature and specific humidity show continuous increases from January to 28.4°C and 21 g/kg in May. Also, mean relative humidity peaks in May at 95%, with lower values observed during the northeast monsoon and the early first non-monsoon (December to April), reaching a minimum of 49.2% in January. From late May, specific humidity gradually declines, stabilizing after mid-July until October with levels ranging from 16 g/kg to 20 g/kg. Significant oscillations occur during the southwest and northeast monsoons, with amplitudes of approximately 1.3 g/kg and 2.3 g/kg, respectively. During the southwest monsoon, temperature, and specific humidity peak in May (monthly averages of 28.4 ± 1.4°C and 21.0 ± 1.1 g/kg). February marks the coldest and driest (specific humidity) month (monthly averages of 27.4 ± 2.6°C and 17.1 ± 1.3 g/kg) during the northeast monsoon (Fig. S3). The seasonal temperature variations exhibit modest amplitudes (Fig. 2), attributed to the tropical climate at Matara station. Conversely, relative humidity displays higher amplitude seasonal than synoptic variations. Furthermore, daily average SSTs consistently exceed the daily average 2m air temperatures recorded by the AWS (Fig. 2).

Yearly averages for water vapor isotopic values are -11.6‰ for $\delta^{18}O$, -79.5‰ for δD, and 13.3‰ for d-excess, respectively. Isotopic composition ranges from -23.9‰ to -7.5‰ for $\delta^{18}O$, -173.2‰ to -53.4‰ for δD, and -1.2‰ to 28.1‰ for d-excess (Table 1). Monthly averages of water vapor isotopes ($\delta^{18}O$ and d-excess) exhibit stability from March to October, followed by sudden decreases. $\delta^{18}O$ and δD show distinct seasonal variations, with higher values during the southwest monsoon and lower values during the northeast monsoon (Table 1). Consequently, the subsequent analysis will concentrate on the variations in $\delta^{18}O$. $\delta^{18}O$ decreases during the southwest, northeast , and non-monsoon periods, with mean values of -11.1‰, -12.2‰, and -11.9‰, respectively. Extreme values of $\delta^{18}O$ are observed during the northeast monsoon, with a maximum of -7.5‰ and a minimum of -23.9‰. Conversely, d-excess exhibits a reverse pattern to $\delta^{18}O$ on both seasonal and monthly scales, characterized by lower values during the southwest monsoon and higher values during the non-monsoon period. Furthermore, d-excess increases during the northeast, southwest, and non-monsoon periods, with mean values of 12.4‰, 13‰, and 14.7‰, respectively. The d-excess maximum occurs in November at 28.1‰ (monthly average of 15.2 ± 4.3‰), while the minimum of -1.2‰ was recorded in January (monthly average of 11.3 ± 4.5‰). d-excess peaks in April 2020 at 19.1‰, indicating potential contributions from local recycling. The high values of d-excess are related to moisture recycling. Low specific humidity corresponds to depleted $\delta^{18}O$ and elevated d-excess, indicating a strong depletion during the long-distance transport from the source regions to the observation station.

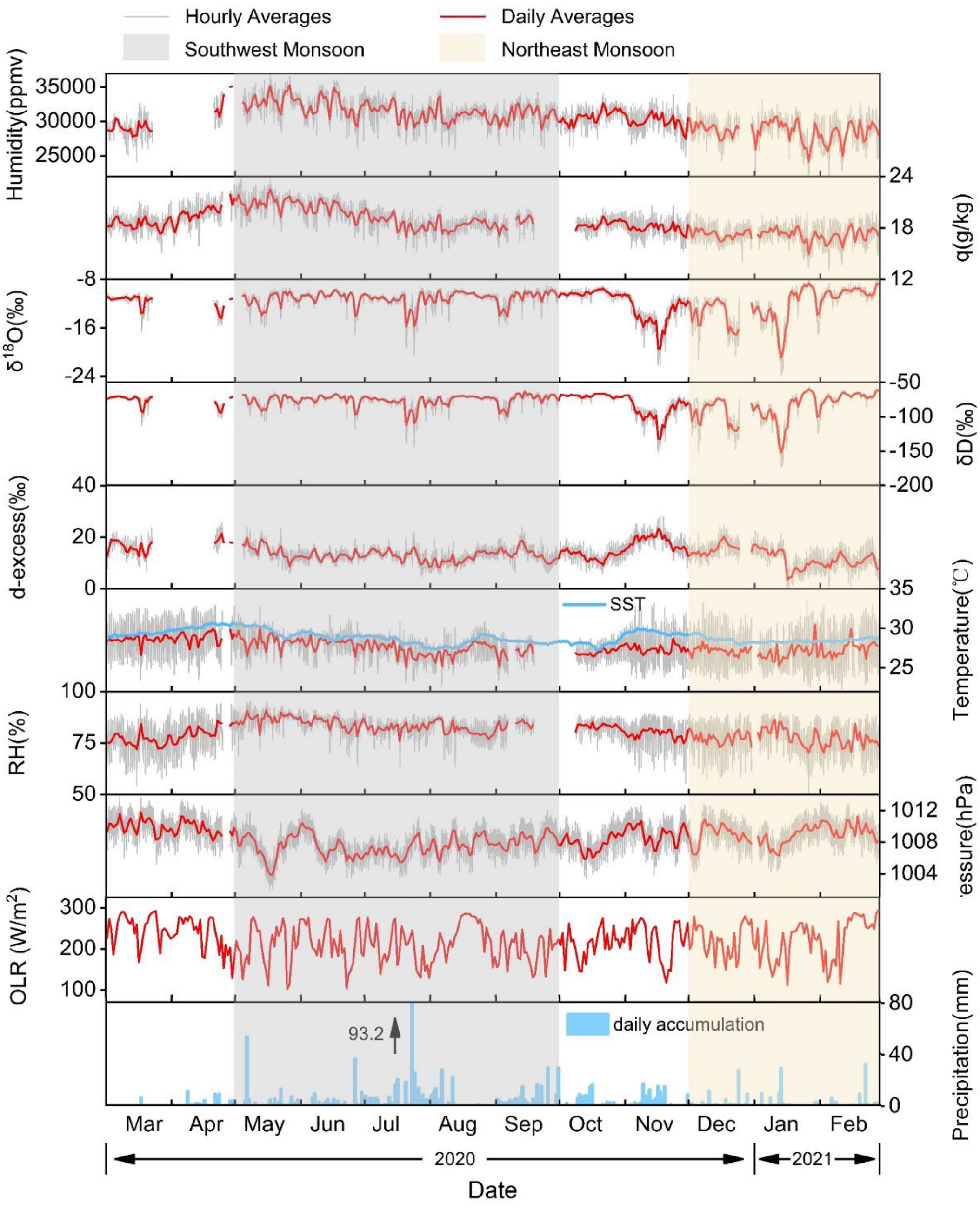

Figure 2: Near-surface observations at Matara station of water vapor isotopes ($\delta^{18}O$, δD, and

d-excess) and meteorological parameters (humidity, specific humidity (q), temperature, relative humidity (RH), pressure, outgoing longwave radiation (OLR, obtained from NCEP), and precipitation) from March 1, 2020, to February 28, 2021. Local sea surface temperature at Matara (SST, obtained from ERA5) is plotted in blue.

Table 1: Summary of hourly-averaged data collected at Matara station from March 1, 2020, to February 28, 2021.Averages are shown in bold. N indicates the number of observations of δ^{18}O, δD, d-excess, temperature (T), relative humidity (RH), specific humidity (q), atmospheric boundary layer height (BLH), and lifting condensation level (LCL). Yearly maxima and minima for each parameter are highlighted using bold italics.

Season		δ^{18}O	δD	d-excess	T	RH	q	BLH	LCL
		(‰)	(‰)	(‰)	(°C)	(%)	(g/kg)	(m)	(m)
Non-monsoon	mean	**-11.9**	**-80.6**	**14.7**	**28.0**	**79.4**	**18.6**	**630.1**	**471.4**
	SD	2.2	16.6	3.8	2.2	7.3	1.3	179.1	204.1
	Max.	-9.0	-65.3	***28.1***	33.2	94.2	23.0	1178.8	1283.1
	Min.	-22.1	-151.1	5.1	23.3	54.2	15.1	***84.4***	98.1
	N	1851	1851	1851	2617	2617	2617	2928	2617
Southwest monsoon	mean	**-11.1**	**-75.7**	**13.0**	**27.6**	**83.8**	**19.4**	**741.4**	**348.7**
	SD	1.3	9.6	2.8	1.5	4.5	1.5	149.0	118.4
	Max.	-9.1	-60.8	24.1	32.7	***95.0***	***23.7***	***1564.4***	938.9
	Min.	-20.4	-143.5	4.5	22.7	63.4	15.1	259.0	***78.5***
	N	3314	3314	3314	3192	3197	3192	3672	3192
Northeast monsoon	mean	**-12.2**	**-85.1**	**12.4**	**27.1**	**77.4**	**17.2**	**516.4**	**524.7**
	SD	3.0	22.0	4.29	2.4	7.8	1.2	139.4	224.0
	Max.	***-7.5***	***-53.4***	25.0	***33.5***	90.0	19.9	1125.7	***1465.6***
	Min.	***-23.9***	***-173.2***	***-1.2***	***22.3***	***49.2***	***13.1***	182.0	192.3
	N	1885	1885	1885	1993	1993	1993	2160	1993
All	mean	**-11.6**	**-79.5**	**13.3**	**27.6**	**80.7**	**18.6**	**648.7**	**434.8**
	SD	2.2	16.1	3.6	2.0	7.0	2.1	181.3	195.1
	Max.	-7.5	-53.4	28.1	33.5	95.0	23.7	1564.4	1465.6
	Min.	-23.9	-173.2	-1.2	22.3	49.2	13.1	84.4	78.5
	N	7050	7050	7050	7802	7807	7807	8760	7802

For $\delta^{18}O$, δD, and d-excess, synoptic variations were recorded (Fig. 2). Abrupt changes occurred in late July 2020 and from November 2020 to January 2021, associated with synoptic events. Cumulative precipitation i July 2020 reached 451.8 mm, with a notable rainfall event in late July recording daily rainfall of 93.2 mm. Isotopic $\delta^{18}O$ values show a sharp depletion from -10.4‰ to -20.4‰ within 20 h of isolated rainfall events, lasting for 6 days. Over the 75-day period spanning from late southwest monsoon to mid-northeast monsoon, significant fluctuations can be seen in isotopic δ between -22‰ and -11‰. During the southwest monsoon from July 12 to August 7, $\delta^{18}O$ values varied from -20.4‰ to -9.2‰, and δD values ranged from -143.5‰ to -68.6‰. This finding is consistent with water vapor isotopic $\delta^{18}O$ (-14.1‰ to -9.8‰) and δD (-97.2‰ to 69.1‰) values measured from July 12 to August 7, 2012, near the Bay of Bengal, although the local minimum at Matara station is below the minimum in the Bay of Bengal (Midhun et al., 2013). Other coastal stations such as Bangalore, Ponmudi, and Wayanad also exhibit water vapor isotopic depletion in autumn and winter, mirroring observations at Matara (Table 2).

The atmospheric water vapor line serves as an indicator of the humidity conditions at the vapor source and the fractionation processes along the transport path. The slope reflects the extent of vapor kinetic fractionation, while the intercept indicates the humidity levels at the vapor source. Comparing the Local Meteoric Water Line (LMWL) for $\delta^{18}O$ and δD with the Global Meteoric Water Line (GMWL) we obtain a slope of < 8 during both monsoon periods (Fig. 3a). Seasonal variations are also visible in $\delta^{18}O$ and δD distribution patterns. Daily averages of water vapor isotopic $\delta^{18}O$ and δD demonstrate a strong correlation ($r = 0.96$, slope = 7.26) with a lower intercept at 4.68. During the northeast monsoon, LMWL slope and intercept are higher compared to other periods, indicating significant moisture recirculation. During the southwest monsoon, both the slope (6.93) and intercept (1.18) are lower compared to other periods, correlating with higher rainfall (Fig. 2).

Table 2: Summary of observed water vapor isotope concentrations at various stations in India and the Bay of Bengal.

Country or region	Station or location	Latitude (N°)	Longitude (E°)	Date	$\delta^{18}O$ (‰)	δD (‰)	d-excess (‰)	References
India	Bangalore	13.01	77.55	Jun 1, 2012, to Sep 30, 2012	-23.8 to -9.0	-178.3 to -58.6	-4.5 to 32.7	(Rahul et al., 2016b)
				Oct 1, 2012, to Feb 28, 2013	-22.7 to -10.2	-177.1 to -73.7	-9.5 to 41.4	
	Kolkata	22.56	88.41	May 3, 2019, to Oct 25, 2019	-16.9 to -10.0	-128.3 to -72.8	-7.1 to 25.4	(Bhattacharya et al., 2021)
	Roorkee	29.87	77.88	Feb 1, 2007, to May 31, 2007	-17.0 to -3.0	none	32.0 to 70.0	(Saranya et al., 2018)
				Jun 1, 2007, to Sep 30, 2007	-32.0 to -6.0		40.0 to 87.0	
				Oct 1, 2007, to Dec 31, 2007	-30.0 to -7.0		30.0 to 60.0	
	Ponmudi	8.76	77.12	Apr 1, 2012, to Nov 30 2012	-24.1 to -8.6	-170.0 to -51.0	6.3 to 26.5	(Lekshmy et al., 2018)
	Wayanad	11.51	76.02		-20.5 to -7.9	-139.1 to -50.0	13.3 to 31.2	
	Ahmedabad	23.03	72.56	Apr 1, 2007, to Apr 1, 2008	-19.2 to -8.9	-128.1 to -59.8	6.9 to 40.4	(Srivastava et al., 2015)
	Chhota Shigri	32.58	77.58	none	-19.4 to -10.3	-101.5 to -29.2	28.0 to 62.0	(Ranjan et al., 2021)
Bay of Bengal	6m	none		Jul 1, 2012, to Aug 1, 2012	-13.6 to -10.0	-94.0 to -68.3	5.7 to 16.4	(Midhun et al., 2013)
	25m				-14.1 to -9.8	-97.2 to -69.1	6.9 to 19.4	
	25m			Nov 15, 2013, to Dec 1, 2013	-19.9 to -11.0	-136.6 to -69.4	13.3 to 31.0	(Lekshmy et al., 2022)

We found a significant negative relationship between d-excess and $\delta^{18}O$, with a rate of change for d-excess with $\delta^{18}O$ is -0.68 ‰/‰ (r = -0.55) (Fig. S4a). This is below the -0.05 ‰/‰ recorded at Bangalore station (Rahul et al., 2016b). Seasonally, the correlation between both variables weaken during the southwest , northeast , and non-monsoon periods, with respective rates of change of -0.94 ‰/‰ (r = -0.49), -0.69 ‰/‰

(r = -0.54), and -0.65 ‰/‰ (r = -0.44). Similar patterns are detected for temperature–d-excess and specific humidity–d-excess correlations, showing gradual increases in the slopes and intercepts of the water vapor line. Moreover, the concentrated distribution of vapor values during the southwest monsoon and the highly scattered distribution during the northeast monsoon are indicative of the corresponding seasonal distributions of the water vapor line.

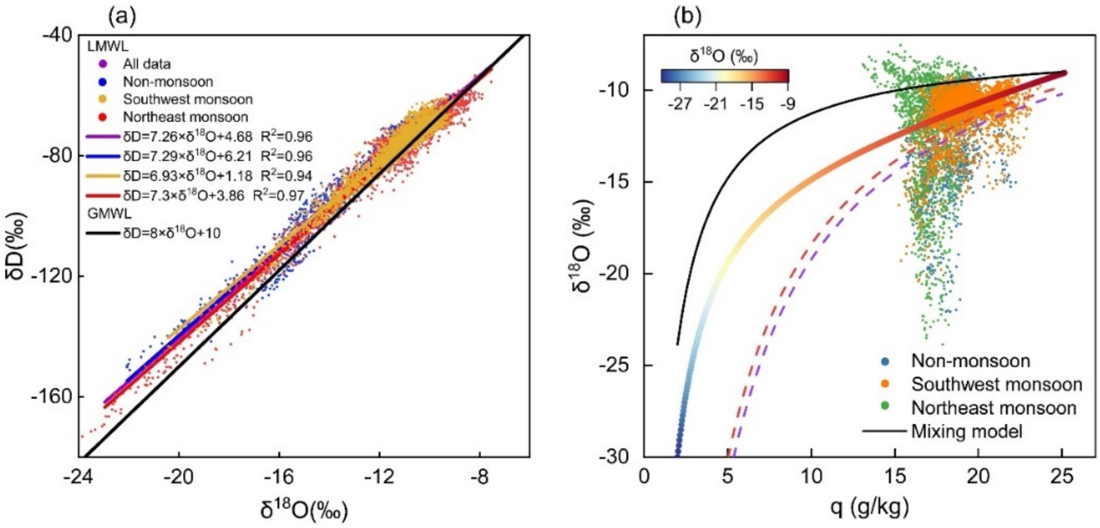

Figure 3: (a) Co-variation of water vapor isotopic composition and meteorological parameters during different monsoon and non-monsoon periods between March 1, 2020 and February 28, 2021. The lines represent linear least-squares regressions (LMWL and GMWL) of δD (‰) as a function of $\delta^{18}O$ (‰). (b) Scatter plot of observed hourly water vapor isotopic $\delta^{18}O$ vs. specific humidity (q). The dashed red and blue curves represent the Rayleigh distillation line during the southwest and northeast monsoon. The solid black curve represents the mixing line. The colored curve represents the MBL-mixing line.

Plots of q-$\delta^{18}O$, the theoretical Rayleigh distillation curve, the mixing-line, and MBL-mixing curve, were used to assess mixing conditions during the study period (Fig. 3b). During the southwest monsoon, most measurements are clustered between the Rayleigh and mixing curve, indicating isotopic variability dominated by leaching effects of precipitation and moisture mixing process. Limited water vapor measurements are scattered below the Rayleigh fractionation line, implying a discernible impact of raindrop re-evaporation. Similarly, during the non-monsoon period, most measurements lie between the Rayleigh and mixing curves, with only a few located below the Rayleigh line. During the northeast monsoon, $\delta^{18}O$ spans from the upper to the lower extreme of the mixing and Rayleigh distillation curves. The measurements substantially deviate from the Rayleigh curve and show a higher depletion than predicted by the Rayleigh model, likely due to the influence of convective processes.

3.2 Diurnal Cycles

To look for diurnal cycles in isotopic composition and meteorological parameters, we analyzed hourly averages (Fig. 4c-e).

All isotopic ($\delta^{18}O$, δD, and d-excess) and meteorological parameters exhibit strong diurnal variations during both monsoon and non-monsoon periods (Fig. 4). Overall, the diurnal variations in local meteorological parameters solar radiation during the day and the resulting development of a boundary layer, with increasing temperatures and wind speeds between noon and the afternoon, accompanied by a decrease in relative humidity due to significant evapotranspiration. At night, surface radiative cooling causes temperatures to drop, resulting in calmer conditions near the surface and gradual air saturation, indicating a relatively stable atmospheric boundary layer. During the southwest monsoon, $\delta^{18}O$, δD, relative humidity, wind speed, specific humidity, and BLH are generally higher than during the northeast and non-monsoon periods, while d-excess and LCL are lower. In the early morning, $\delta^{18}O$ steadily decreases, reaching a minimum (-11.26‰) around sunrise (~09:00 local time (LT)). Subsequently, it increases throughout the day, peaking (-10.87‰) in the afternoon (~15:00 LT), yielding a diurnal fluctuation of merely 0.45‰. Increased specific humidity between 10:00 LT and 14:00 LT coincides with increasing air temperatures and wind speeds and decreasing relative humidity (Fig. 4c-f). BLH peaks between 14:00 LT and 16:00 LT, slightly later than other meteorological parameters. The same diurnal variations for each parameter were observed during the northeast monsoon, with maximum changes in $\delta^{18}O$ and d-excess of 1.1‰ and 6.8‰, respectively. Specific humidity peaks between 10:00 LT and 16:00 LT, accompanied by increases in air temperature, wind speed, BLH, and LCL. After 16:00 LT, specific humidity decreases alongside isotopic δ values and other meteorological parameters. d-excess peaks (14.81‰) at 09:00 LT and fluctuates until 23:00 LT, contrasting with the period from 04:00 LT to 09:00 LT (Fig. 4b). d-excess exhibits a W-shaped variability, reaching similar highs at 09:00 LT and 21:00 LT. Specific humidity exhibits a diurnal variation that aligns closely with the $\delta^{18}O$ pattern, reaching its minimum before sunrise and peaking around midday (10:00-15:00 LT). Between afternoon and evening, specific humidity remains relatively high and stable. The diurnal variation during the southwest and northeast monsoon periods are 1.28 g/kg and 2.32 g/kg, respectively. Similarities with patterns observed at Lena station (Bonne et al. 2020) suggest potential influences from moisture exchange between the atmosphere and ocean surface, particularly during the northeast monsoon.

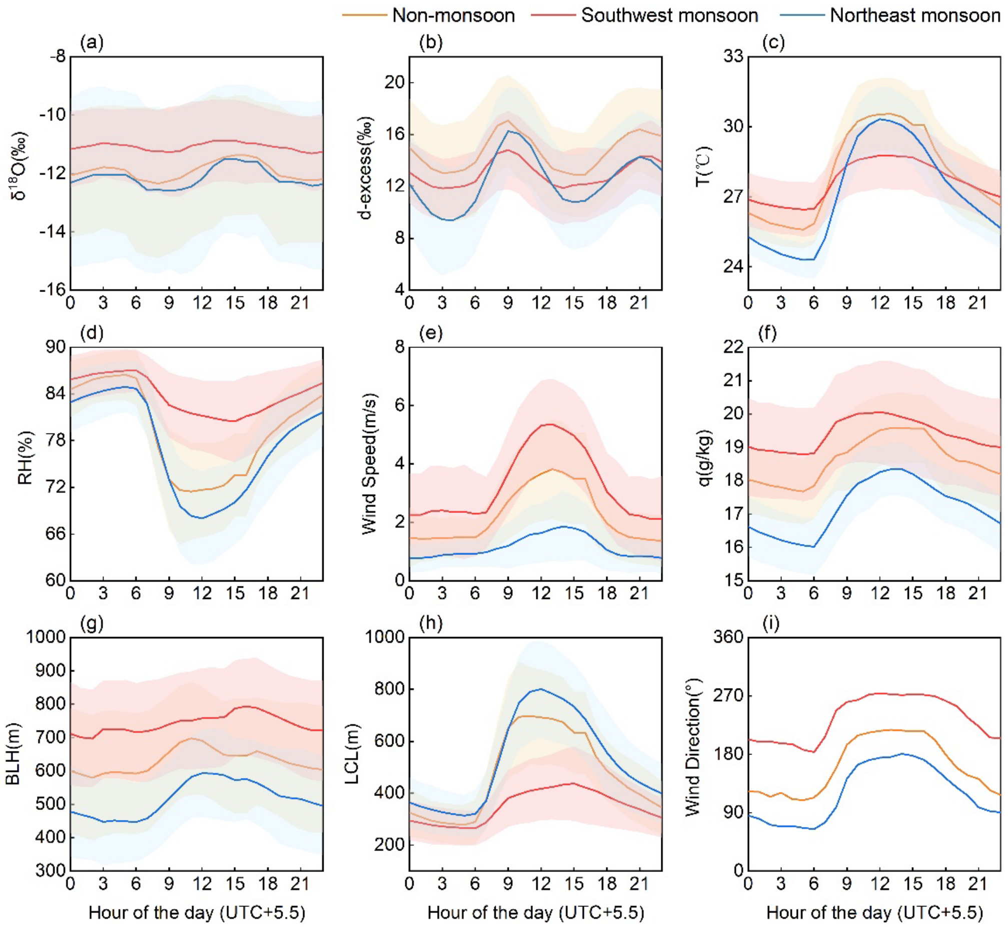

Figure 4: Average diurnal cycles of (a) $\delta^{18}O$, (b) d-excess, (c) temperature (T), (d) relative humidity (RH), (e) wind speed, (f) specific humidity (q), (g) atmospheric boundary layer height (BLH), (h) lifting condensation level (LCL), and (i) wind direction during the non-monsoon, southwest monsoon, and northeast monsoon periods. Shaded areas correspond to

±1 standard deviation.

3.3 Sea Surface Evaporation Conditions in the Moisture Source Region

To be able to explore water vapor isotopic variations in the sea surface boundary layer, we must first understand the processes and factors that affect isotope variations during ocean surface water evaporation. The primary determinant governing water vapor stable isotope shifts across different regions is the regional moisture transport process, characterized by differences in isotopic variations in the moisture source region, variations in meteorological conditions during the evaporation processes, and divergences of the moisture transport pathways (Bonne et al., 2020). Thus, this section aims to identify factors that drive the seasonal variations of near-surface atmospheric water vapor stable isotopes at Matara, including water vapor origin, transmission routes, and sea surface evaporation conditions in the source regions.

To further understand the different seasonal relationships between $\delta^{18}O$, d-excess, and meteorological parameters, we analyzed potential seasonal differences between the main moisture sources using HYSPLIT. Trajectories that reach Matara during the southwest and northeast monsoons have different origins. During the southwest monsoon, wind directions span from 60° to 360° and the main origin regions are therefore the Arabian Sea (AS) and Indian Ocean (Fig. 5a). Due to the northward movement of the warm South Equatorial Current, these winds gather significant amounts of moisture along the way, bringing heavy rainfall to Matara (Fig. 5a). Conversely, during the northeast monsoon, the main wind direction shifts to 0°-225° and 330°-360°, such that most trajectories originate in northeast India, where specific humidity is lower (overland), and only a short portion of the trajectory passes over the BoB. The long transport distance results in a greater depletion in water vapor isotopes once the air mass arrives at Matara station.

Moisture from all sources shows seasonal variations, with $\delta^{18}O$ values lower during the southwest monsoon than during the northeast monsoon. The shift in water vapor source from the AS in May to the southern Indian Ocean in September leads to

$\delta^{18}O$ enriched water vapor from August to September. Enhanced convective activity and rainfall during the southwest monsoon result in $\delta^{18}O$ depletion, while tropical storms and hurricanes also contribute to $\delta^{18}O$ depletion.

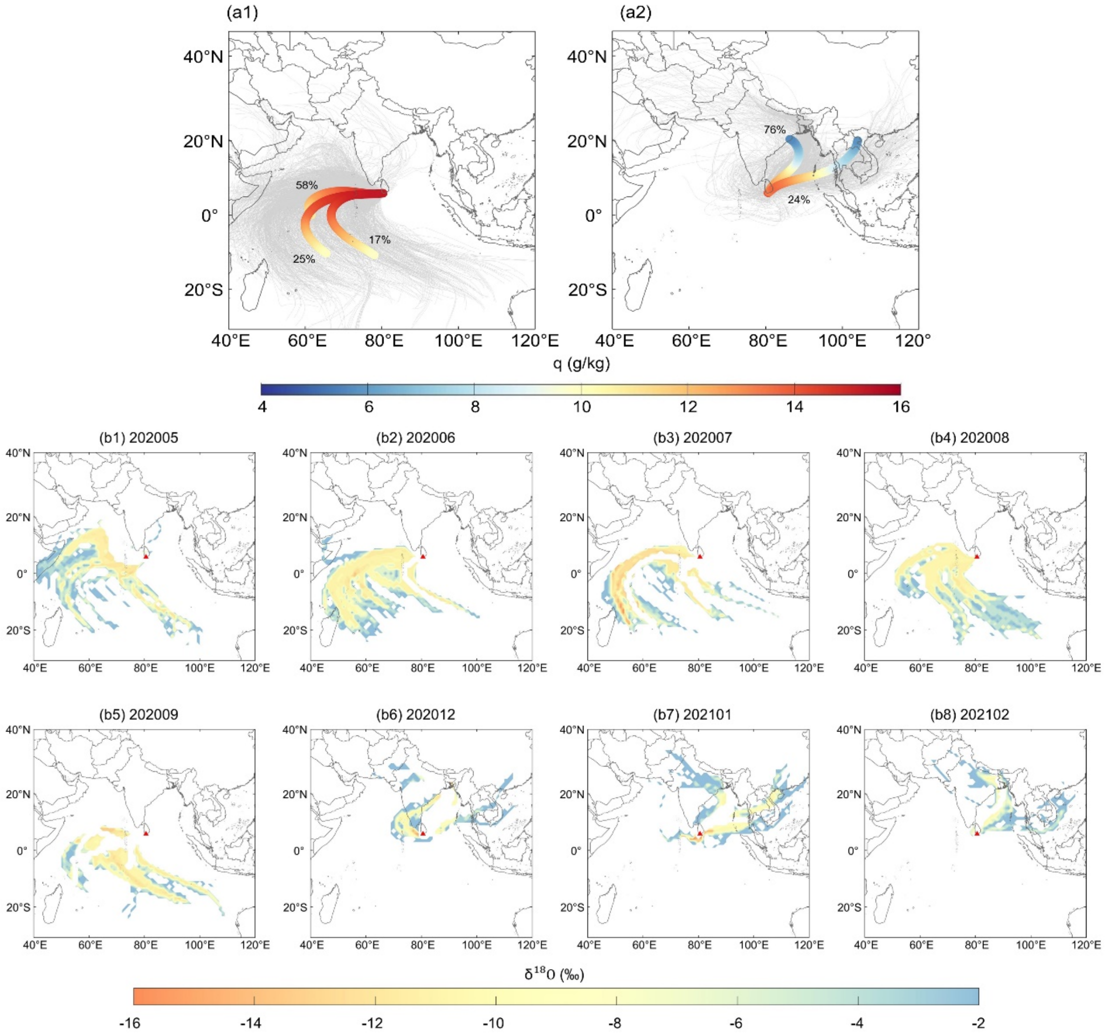

Figure 5: Backward trajectories of water vapor tracks reaching Matara station and its four surrounding sites (height: 50m, 500m, 1200m, and 2000m) during the (a1) southwest monsoon and (a2) northeast monsoon. The changes in specific humidity (q) along each clustered trajectory are shown in color. Numbers indicate the proportion (%) of trajectories represented by each clustered trajectory. Monthly concentration fields of water vapor isotopic $\delta^{18}O$ from a 168h HYSPLIT simulation of back trajectories during the two monsoon seasons (b1-b8). Red triangle marks the study site.

d-excess exhibits similar seasonal variations at Matara station, with lower values during the two monsoon seasons and higher values during the non-monsoon periods

(Table 2, Fig. 4). This seasonal variation may stem from changes in relative humidity in the moisture source areas and further modifications during transport.

Ocean evaporation represents the starting point of the phase transformations that occur within the global water cycle. Identifying the isotopic variations and controlling factors of oceanic evaporation is essential for understanding isotopic shifts in the marine boundary layer. Previous coastal observational studies focusing on the marine boundary layer have confirmed a significant association between d-excess and RH_{SST} (Pfahl and Wernli, 2009; Steen-Larsen et al., 2015). In cases where dynamic fractionation during air mass transport is either absent or minimal, d-excess can serve as an indicator of the moisture source region (Bonne et al., 2014).

The map of the moisture sources (Fig. 5) identified the Indian Ocean and BoB as the main source areas for moisture arriving at Marara station. To gauge the impact of more local influences, we investigated how changes in sea surface meteorological conditions in the sea around Matara station affects near surface water vapor isotope concentrations (Fig. S6). During the southwest monsoon, RH_{SST} in "Region a" (located to the south of Matara between 3-6°N and 78-82°E) ranged from 66% to 84%, with SST fluctuating between 28.0°C and 30.6°C. During the northeast monsoon, RH_{SST} in "Region b" (located to the east of Matara between 6-8°N and 82-85°E) ranged from 54% to 84%, with SST fluctuating between 28.1°C and 29.1°C. In comparison with the southwest monsoon, RH_{SST} is slightly lower, accompanied by less pronounced variability in SST. The rate of change in d-excess under the influence of RH_{SST} in the BoB (during the northeast monsoon) is -0.34 ‰/%. In comparison, the rate of change in d-excess with the RH_{SST} of the northern Indian Ocean (during the southwest monsoon) is -0.51 ‰/%, suggesting that evaporation over the northern Indian Ocean significantly impacts local d-excess. Studies focused on the BoB 's sea surface revealed that RH_{SST} explains only 25% of the d-excess variation (d-excess = $(-0.55 \pm 0.14) \times RH_{SST} + (56 \pm 12)$; r = -0.5). The limited variation in relative humidity during the monsoon period led to a low correlation, indicating that monsoon moisture plays a crucial role in the isotopic composition of water vapor in the BoB (Midhun et al., 2013). Conversely, the observed relationship between near-surface water vapor d-excess at Matara and relative humidity in the surrounding oceanic region during the observational period, with correlation coefficients of -0.61 and -0.62 ($p<0.01$), respectively (Fig. 6), reveals a marked negative correlation between d-excess and relative humidity in the nearby Indian Ocean and BoB, indicating that water vapor at Matara is predominantly supplied by nearby oceans. Notably, SST amplitude near the Matara station is smaller than the variations in near-surface air temperature (Fig. 2).

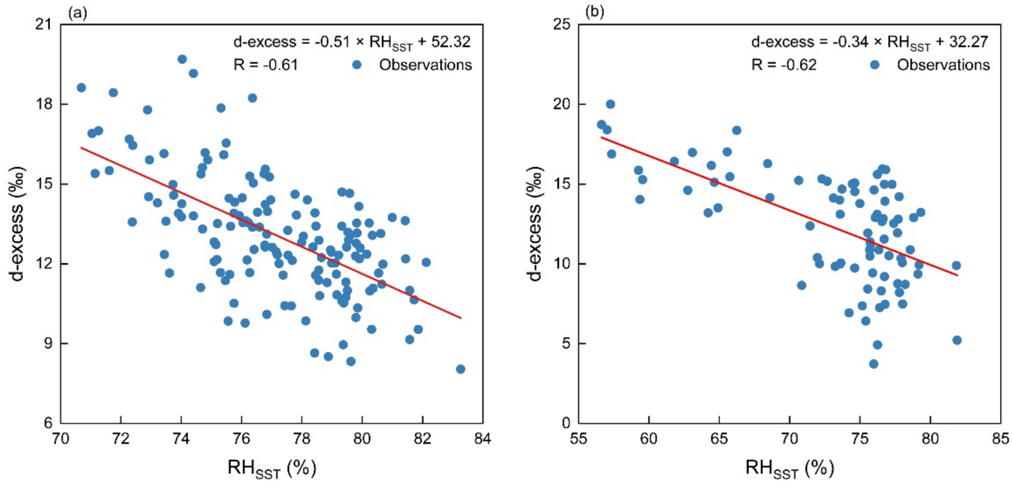

Figure 6: Relationship between d-excess and RH$_{SST}$ during the (a) southwest monsoon and (b) northeast monsoon. Specific sea regions (Fig. S6) to the south (Region a: 3-6°N and 78-82°E) and east (Region b: 6-8°N and 82-85°E) of the observation station were selected to investigate the impact of sea surface meteorological conditions on near-surface water vapor isotopes during the two monsoon periods.

3.4 Influence of Convective Activity

In the equatorial tropics, OLR mainly results from convective activity and cloud cover, which can impact the stable isotope composition of precipitation (Ohring et al., 1984; Gao et al., 2013; Guo et al., 2017). Generally, higher OLR values are associated with weaker convective activity. Examining the correlation between stable isotopes of water vapor and OLR helps to understand the impact of convective activities along near-surface trajectories of water vapor stable isotopes at Matara station.

We calculated the spatiotemporal correlation between OLR and precipitation amount using the measured water vapor isotopic compositions at Matara station.

Specifically, we calculated the average precipitation amount for each grid point by averaging over different numbers of days (n = 1, 2, up to 30) preceding each precipitation day. Lower OLR values indicate the presence of deep convective clouds in this region and higher precipitation associated with lower δ values.

Fig. 7a shows the strong positive correlation (red regions) between rainfall and $\delta^{18}O$ during the southwest monsoon, mainly in the northern BoB and over India. This correlation strengthens and extends over wider areas as n increases from 1 to 5. Additionally, a strong negative correlation is evident in the northern Indian Ocean and southern Arabian Sea, reaching a maximum for n = 2 d. During the northeast monsoon, the spatial correlation distribution differs, with a negative correlation observed over the southern Indian Ocean and BoB (Fig. 7b). Lower OLR values in the Arabian Sea, the southern part of the BoB, and throughout Southeast Asia correspond to a decrease in water vapor isotopic $\delta^{18}O$ at Matara station (Fig. 7c, d). This pattern indicates that water vapor $\delta^{18}O$ during the northeast monsoon period is influenced by convective activities over the Arabian Sea, South BoB, and Southeast Asian regions. The stronger this convective activity, the more depleted is the air reaching Matara in water vapor isotopic $\delta^{18}O$.

To examine the correlation between water vapor isotopic $\delta^{18}O$ and local precipitation (Fig. 7e) and OLR (Fig. 7f), we selected a small region of 5°×5° around Matara and calculated the time- and space- correlation for all grid points as described above. The results show that the correlation with precipitation is negative during both monsoon seasons as expected. The depletion of low-level water vapor $\delta^{18}O$ is related to the transport and deposition of water vapor into the lower atmosphere through convective activity (Kurita, 2013; Midhun et al., 2013; Lekshmy et al., 2014). The air masses are re-supplied to the convective system through moisture recycling. This results in a strong correlation between the isotopic composition of water vapor and the convective activity during the previous day (Fig. 7, f). Residual water vapor is more depleted in strong convective systems. In our study, the correlation reaches a high value after about 5 days, indicating that the convective activity is sufficiently established to affect the isotopic composition of water vapor. In fact, the correlation (for $p < 0.05$ and in absolute terms) is high for all n values, with maxima of about 0.48 for n = 3 d during the southwest monsoon and 0.72 for n = 4 to 9 d during the northeast monsoon.

The OLR correlation peaks at smaller time scales(approximately n = 1-4 d, Fig. 7f) than precipitation(n = 3-8 d). We attribute this difference to the effect of cloud distribution on precipitation and OLR. OLR has a stronger response to shallow clouds, while precipitation is more responsive to both deep convective clouds and shallow clouds (Masunaga and Kummerow, 2006; Schumacher, 2006). The OLR minimum occurs when thunderstorm clouds result in more precipitation. Additionally, deep thunderstorm clouds, with short lifetimes and consequently very low OLR (corresponding to highly depleted water vapor isotopic δ), exhibit a short memory effect on the correlation (peak occurs at smaller time scales) (Gambheer and Bhat, 2000).

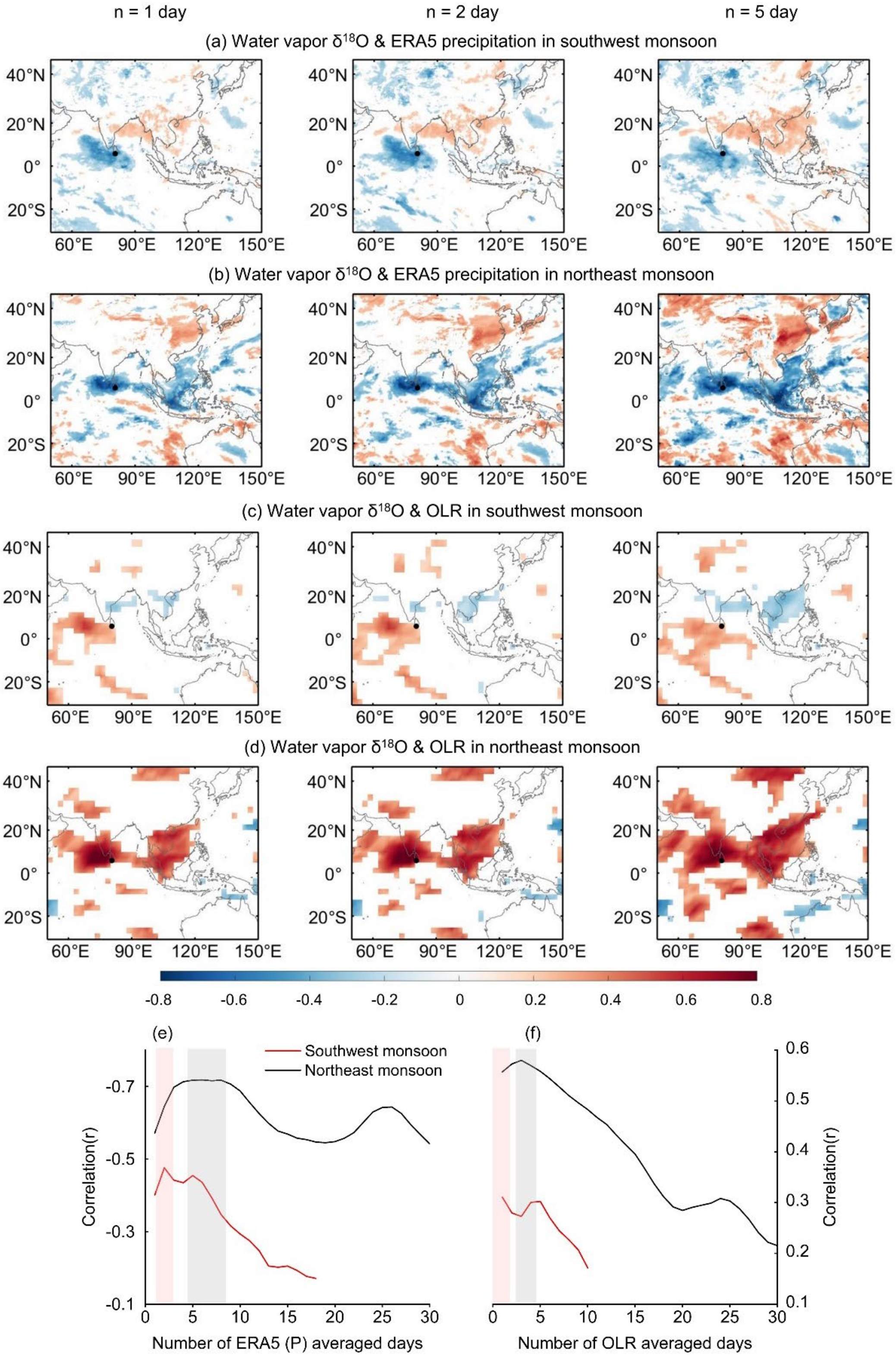

Figure 7: Spatial correlation fields of water vapor isotopic composition and averaged ERA5 precipitation (P) during the (a) southwest monsoon and (b) northeast monsoon, along with the spatial correlation fields for average outgoing longwave radiation (OLR) during the (c) southwest monsoon and (d) northeast monsoon. Averaging was conducted at each grid point

for three periods of n = 1, 2, and 5 d preceding each of the 153 days of the southwest monsoon (a, c) and 90 days of the northeast monsoon (b, d). Correlation between (e) $\delta^{18}O$ and P, as well as (f) $\delta^{18}O$ and OLR during the southwest monsoon (red line) and northeast monsoon (black line) n = 1, 2, 3, … 30 d. Red (grey) areas show the n-range for which the highest correlation was obtained during southwest (northeast) monsoon. Here, n represents the average "moisture mixing time" of regional precipitation, affecting water vapor isotopes through the transport of residual water vapor (Rahul et al., 2016b).

During both the southwest and northeast monsoons, $\delta^{18}O$ exhibits a weak correlation with 2m air temperature (Fig. S7) for the simultaneous values. Throughout the year, the relationship between 2m air temperature and $\delta^{18}O$ in water vapor is $\delta^{18}O = 0.7T – 30.8$ ($r = 0.32$) (Fig. S9). During the southwest and northeast monsoons, the relationships become $\delta^{18}O = 0.5T – 24.95$ ($r = 0.39$) and $\delta^{18}O = 1.46*T – 51.71$ ($r = 0.43$), respectively (Fig. S7). Daily temperature and $\delta^{18}O$ values fluctuate less during the southwest monsoon than during the northeast monsoon (Fig. 4), possibly due to a weaker temperature inversion during the southwest monsoon.

The correlation between $\delta^{18}O$ and relative humidity differs between the two monsoon periods. During the southwest monsoon, $\delta^{18}O$ and relative humidity appear uncorrelated ($r = 0.01$), consistent with previous findings (Rahul et al., 2016b). Conversely, during the northeast monsoon, a robust negative correlation emerges between $\delta^{18}O$ and relative humidity ($r = -0.58$). Similarly, the relationship between $\delta^{18}O$ and precipitation varies between both monsoon seasons (Fig. S7). Moreover, during the southwest monsoon, heavy precipitation leads to relatively high relative humidity and the enrichment of heavier isotopes.

4. Discussion

This study presented the results from a one-year (March 2020 to February 2021) in-situ measurement campaign of near-surface atmospheric water vapor isotopes ($\delta^{18}O$, δD) at Matara station, Sri Lanka. These high-temporal resolution water vapor isotopic composition and meteorological observations provided a good opportunity to investigate the water vapor isotopic dynamics from synoptic to seasonal scales. The variability of water vapor isotopes at Matara station is influenced by local meteorological factors, oceanic evaporation processes, and regional convective activities, depending on the water sources and moisture transport. The measurements provided insights into multi-time-scale variations in near-surface atmospheric water vapor in an equatorial region and provided information about the interactions between large-scale atmospheric moisture transport and oceanic evaporation.

4.1 Seasonal Versus Synoptic Variabilities and Water Vapor Flux

To evaluate the influence of seasonal variations in moisture sources on the stable water vapor isotopic composition, we focus on how changes in specific humidity and isotopes relate to observed variations in wind direction at Matara station (Fig. S11). During the southwest monsoon, the distribution of wind directions appears relatively narrow, and the highest specific humidity values were recorded for west-north-westly (WNW) wind directions (Fig. S11). $\delta^{18}O$ values were highest and d-excess lowest if the moisture source area was to the west of Matara, while $\delta^{18}O$ depletion and high d-excess were associated with air masses that arrived from the east (Fig. S11). The southwest monsoon period exhibits similar ranges of specific humidity and water vapor isotope composition irrespective of wind direction. During the northeast monsoon, the northeastern winds from BoB brings a higher proportion of more dry air, resulting in the range of specific humidity between 14 and 17 g/kg (Fig. S11) and isotopically depleted water vapor ($\delta^{18}O < -22‰$) compared to other regions. Thus, these air masses undergo considerable isotopic fractionation as they pass overland before reaching our measurement site. For air masses originating in the southeast and northwest, isotopic composition may be influenced by closer moisture sources, associated with the considerable moisture uptake observed over the Arabian Sea and northern Indian Ocean (Fig. S12). With easterly and northeasterly winds $\delta^{18}O$ is often elevated, with $\delta^{18}O$ (exceeding -10‰) associated with the northwesterlies (Fig. S11).

Since the local wind direction only provides information on the final stage of air mass transport, we conduct a more detailed analysis of how water vapor flux, evaporation, and precipitation along the transport pathway affect local variations in stable water vapor isotopes. During the southwest monsoon, evaporation rates at Matara station are lower than precipitation rates (Fig. S12), something we also observed over the central Indian Ocean. In contrast, over the northern Indian Ocean and western BoB, located up and downstream from Matara station, we obtained a water vapor budget where evaporation exceeded precipitation. During the northeast monsoon, the Matara region is affected by moisture sources from the BoB and South Asia, resulting in higher evaporation rates than precipitation rates and an increase in water vapor flux. In summary, the monthly variations in water vapor flux and budget indicate significant differences in moisture transport between the southwest and northeast monsoons. The upstream water vapor budget significantly affects the changes on stable water vapor isotopes, particularly $\delta^{18}O$. During the southwest monsoon, there is a clear increase in precipitation, with moisture transport primarily arriving from the northeast. During this period, evaporation in the upstream region exceeds precipitation, suggesting a higher water vapor content along the transport pathway, which corresponds to a continuous enrichment of $\delta^{18}O$ at Matara station. In contrast, during the northeast monsoon, moisture transport is mainly from the southwest. From December 2020 to January 2021, upstream precipitation exceeded evaporation, leading to a “washing effect” where water vapor continuously undergoes condensation and fractionation due to precipitation along the transport pathway, resulting in a gradual depletion of $\delta^{18}O$.

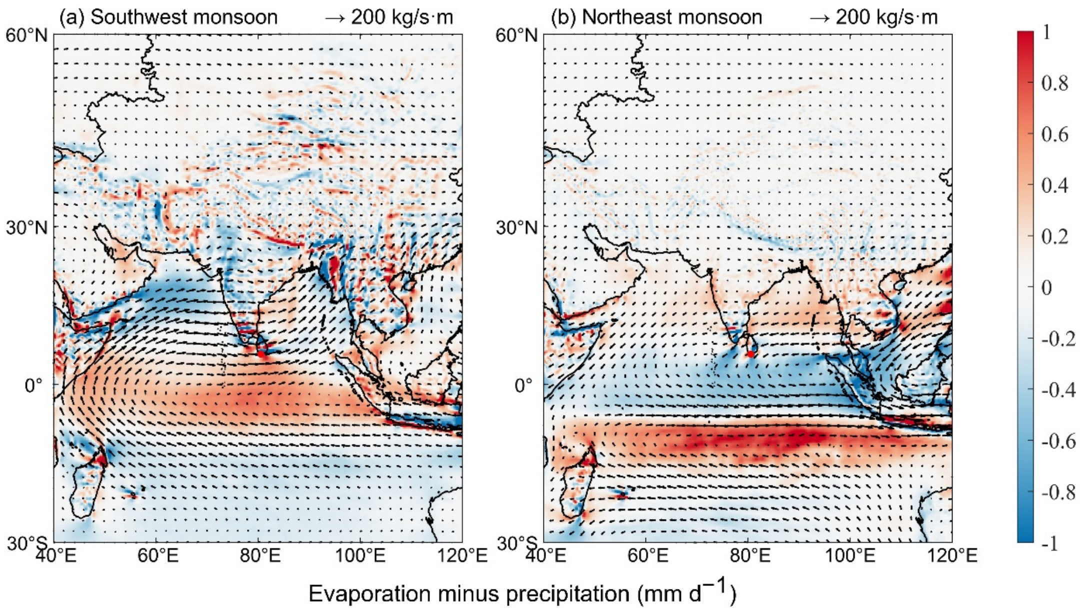

Figure 8: Comparing average water vapor flux and water vapor budget during the (a) southwest monsoon and (b) northeast monsoon. The red dot indicates the location of Matara station.

4.2 Comparing Main Features and Identifying Influencing Factors

During the both monsoon periods, specific humidity and stable water isotope composition showed a clear diurnal cycle at Matara station, primarily due to the significant contribution of local evapotranspiration to the overall moisture balance. In equatorial regions, seasonal variations in stable water vapor isotopes are largely governed by changes moisture sources and the transport processes. Ponmudi station, located in southern India (Lekshmy et al., 2018), shares many characteristics with Matara station, in that it is also a coastal city, influenced by both the southwest and northeast monsoons. During the summer, moisture sources for air arriving at Ponmudi are mostly located in the southern Arabian Sea and equatorial Indian Ocean, with relative humidity levels exceeding 70%. This high relative humidity, combined with a continuous supply of moisture from the Arabian Sea, results in significant rainfall in the Ponmudi region, exceeding 2040 mm.

Fluctuations of water vapor stable isotopes at shorter (weather) time scales are closely associated with regional convective activities. Research conducted on precipitation and water vapor stable isotopes at Bangalore, another coastal city in southern India, indicates that local meteorological parameters do not influence isotope ratios (Rahul et al., 2016b). Rather, these ratios are affected by the integrated regional convective activity, characterized by large-scale rainfall or outgoing longwave radiation flux. Like Matara station, Bangalore is also affected by both the southwest and northeast monsoons. The observed depletion in heavy isotopes may be due to the influx of moisture from the Bay of Bengal, depleted due to the rainout effect, mixing with air that has travelled overland crossing the Indian subcontinent.

Overall, the long-term monitoring of water vapor stable isotopes in South Asian equatorial regions could highlight the importance of both seasonal and sub-seasonal (weather-scale) variations, mostly due to changes in moisture sources and processes that occur during the air mass transport at the circulation scale. Matara station served as a good location to study the effects of moisture transport processes over the Indian Ocean. We could also identify seasonal patterns that general agreement with previous findings for tropical equatorial regions (Midhun et al., 2013; Rahul et al., 2016b; Lekshmy et al., 2018).

5. Summary and Conclusions

One-year (March 2020 to February 2021) in situ meteorological observations and measurements of water vapor isotopic composition were conducted at Matara station, Sri Lanka. Meteorological parameters exhibited diurnal variations during both monsoon and non-monsoon periods. During the northeast monsoon, diurnal fluctuations in $\delta^{18}O$, temperature, and specific humidity were observed, with maximum values reaching 1.1‰, 6.0°C, and 2.3 g/kg, respectively. In contrast, during the southwest monsoon these parameters exhibit only small magnitude fluctuations of 0.45‰, 2.3°C, and 1.3 g/kg. Atmospheric temperature affects isotopic composition through its effect on isotope fractionation. Additionally, a weak seasonal variability in near-surface water vapor isotopes was observed, with $\delta^{18}O$ typically showing high values (-11.1‰) during the monsoon period and low values (-11.9‰) during the non-monsoon period. d-excess exhibited lower value (12.7‰) during the monsoon period than during the non-monsoon period (14.7‰).

Evaporation over the northern Indian Ocean significantly impacts local d-excess at Matara. Contrary to previous research indicating a weak correlation ($r = -0.5$) between d-excess in the Bay of Bengal and the sea surface relative humidity (RH_{SST}) (Midhun et al., 2013), we found a slightly stronger negative correlation with RH_{SST} during the monsoon periods, with values of -0.61 and -0.62 ($p<0.01$) for the northern Indian Ocean and Bay of Bengal, respectively. This study underscores the capability of near-surface d-excess to reflect the evaporation conditions over these oceanic source regions.

Consistent with previous research (Rahul et al., 2016b), large-scale rainfall and regional convective activity (OLR) significantly impact isotope ratios at Matara station. Notably, significant changes in $\delta^{18}O$ were observed during a heavy rainfall event in July 2020, with a sharp decline in isotopic values from -10.4‰ to -20.4‰ within 20 hours. During the southwest monsoon, strong cloud cover and high humidity over the ocean may lead to $\delta^{18}O$ enrichment at Matara station. The water vapor isotope compositions observed during the southwest monsoon are similar as those observed in the Bay of Bengal (Midhun et al., 2013). The deficiency of water vapor isotope values at Matara station in autumn and winter is consistent with findings from other coastal stations, such as Bangalore, Ponmudi, and Wayanad (Rahul et al., 2016b; Lekshmy et al., 2018). Our study is the first to point out that the correlation between OLR and $\delta^{18}O$ peaks around 1-4 days, which we attribute to the impacts of cloud distribution.

This study contributes to a better understanding of the origins of moisture arriving at Matara station and the associated atmospheric transport. This comprehensive dataset containing synchronous water vapor isotope and meteorological measurements offer extensive opportunities for further analyses, e.g., of the typical weather events, atmospheric patterns, and ocean-atmosphere interactions in the equatorial region. Nevertheless, additional and continuous observations of water vapor stable isotopes in this region are urgently needed to be able to study interannual variability. Given the anticipated changes in numerous weather and hydrological processes in equatorial regions, future research should explore the impacts of typical weather events, and ocean-atmosphere interactions, to deepen our understanding of extreme events and large-scale atmospheric modes (e.g., ENSO, MJO, and IOD). Considering the temporal and spatial variability in the dynamics of tropical ocean-atmosphere systems, high-resolution isotope models and satellite datasets should be combined for a more comprehensive analysis in the future.

Acknowledgements:

This work was funded by The Second Tibetan Plateau Scientific Expedition and Research (STEP) program (Grant No. 2019QZKK0208) and the National Natural Science Foundation of China (Grants 41922002 and 41988101-03), as well as the Innovation Program for Young Scholars of TPESER (QNCX2022ZD-01). We thank staff in the China Sri Lanka Joint Center for Education and Research, Mr. Charith Madusanka Widanage, and Dr. Di Dai for their invaluable support and assistance with measurements.

Author Contributions:

Yuqing Wu: Data curation, Formal analysis, Writing - Original draft preparation. **Jing Gao:** Data curation, Conceptualization, Methodology, Supervision, Writing - Review and Editing, Funding acquisition. **Aibin Zhao**: Writing - Review and Editing, Project administration. **Xiaowei Niu:** Data curation. **Yigang Liu:** Data curation. **Disna Ratnasekera:** Project administration. **Tilak Priyadarshana Gamage:** Project administration. **Amarasinghe Hewage Ruwan Samantha:** Data curation.

Data availability:

The ERA5 dataset is the latest reanalysis dataset published by the European Centre for Medium-Range Weather Forecasts (ECMWF) (Hersbach et al., 2020) (https://cds.climate.copernicus.eu/cdsapp#!/home). The Global Data Assimilation System (GDAS) has been published by the US National Oceanic and Atmospheric Administration (NOAA) (ftp://arlftp.arlhq.noaa.gov/archives/gdas1/). The water vapor isotopic compositions dataset will be available on the Zenodo research data repository after manuscript publication.

Competing interests:

The contact author has declared that none of the authors has any competing interests.

References

Aemisegger, F., Sturm, P., Graf, P., Sodemann, H., Pfahl, S., Knohl, A., and Wernli, H.: Measuring variations of $\delta^{18}O$ and $\delta^{2}H$ in atmospheric water vapour using two commercial laser-based spectrometers: an instrument characterisation study, Atmos. Meas. Tech., 5, 1491-1511, https://doi.org/10.5194/amt-5-1491-2012, 2012.

Angert, A., Lee, J.E., and Yakir, D.: Seasonal variations in the isotopic composition of near-surface water vapour in the eastern Mediterranean, Tellus B, 60, 674-684, https://doi.org/10.1111/j.1600-0889.2008.00357.x, 2008.

Bailey, A., Aemisegger, F., Villiger, L., Los, S.A., Reverdin, G., Quiñones Meléndez, E., Acquistapace, C., Baranowski, D.B., Böck, T., Bony, S., Bordsdorff, T., Coffman, D., de Szoeke, S.P., Diekmann, C.J., Dütsch, M., Ertl, B., Galewsky, J., Henze, D., Makuch, P., Noone, D., Quinn, P.K., Rösch, M., Schneider, A., Schneider, M., Speich, S., Stevens, B., and Thompson, E.J.: Isotopic measurements in water vapor, precipitation, and seawater during EUREC4A, Earth Syst. Sci. Data, 15, 465-495, https://doi.org/10.5194/essd-15-465-2023, 2023.

Bandara, U., Agarwal, A., Srinivasan, G., Shanmugasundaram, J., and Jayawardena, I.M.S.: Intercomparison of gridded precipitation datasets for prospective hydrological applications in Sri Lanka, Int. J. Climatol., 42, 3378-3396, https://doi.org/10.1002/joc.7421, 2022.

Bavadekar, S.N., and Mooley, D.A.: Use of the equation of continuity of water vapour for computation of average precipitation over peninsular India during the summer monsoon, In: Lighthill, J., Pearce, P.R. (Eds.), Monsoon Dynamics, Cambridge University Press, Cambridge, pp., 261-268, 1981.

Bedaso, Z., and Wu, S-Y.: Daily precipitation isotope variation in Midwestern United States: Implication for hydroclimate and moisture source, Sci. Total Environ., 713, 136631, https://doi.org/10.1016/j.scitotenv.2020.136631, 2020.

Benetti, M., Aloisi, G., Reverdin, G., Risi, C., and Sèze, G.: Importance of boundary layer mixing for the isotopic composition of surface vapor over the subtropical North Atlantic Ocean, J. Geophys. Res. Atmos., 120, 2190-2209, https://doi.org/10.1002/2014JD021947, 2015.

Benetti, M., Lacour, J-L., Sveinbjörnsdóttir, A.E., Aloisi, G., Reverdin, G., Risi, C., Peters, A.J., and Steen-Larsen, H.C.: A Framework to Study Mixing Processes in the Marine Boundary Layer Using Water Vapor Isotope Measurements, Geophys. Res. Lett., 45(5), 2524-2532, https://doi.org/10.1002/2018GL077167, 2018.

Benetti, M., Reverfdin, G., Pierre, C., Merlivat, L., Risi, C., Steen-Larsen, H.C., and Vimeux, F.: Deuterium excess in marine water vapor: Dependency on relative humidity and surface wind speed during evaporation, J. Geophys. Res. Atmos., 119, 584-593, https://doi.org/10.1002/2013JD020535, 2014.

Bershaw, J., Penny, S.M., and Garzione, C.N.: Stable isotopes of modern water across the Himalaya and eastern Tibetan Plateau: Implications for estimates of paleoelevation and paleoclimate, J. Geophys. Res. Atmos., 117, 110, https://doi.org/10.1029/2011JD016132, 2012.

Bhattacharya, S., Pal, M., Panda, B., and Pradhan, M.: Spectroscopic investigation of hydrogen and triple-oxygen isotopes in atmospheric water vapor and precipitation during Indian monsoon season, Isot. Environ. Healt. S., 57, 368-385, https://doi.org/10.1080/10256016.2021.1931169, 2021.

Bonne, J-L., Behrens, M., Meyer, H., Kipfstuhl, S., Rabe, B., Schönicke, L., Steen-Larsen, H.C., and Werner, M.: Resolving the controls of water vapour isotopes in the Atlantic sector, Nat. Commun., 10, 1632, https://doi.org/10.1038/s41467-019-09242-6, 2019.

Bonne, J-L., Masson-Delmotte, V., Cattani, O., Delmotte, M., Risi, C., Sodemann, H., and Steen-Larsen, H.C.: The isotopic composition of water vapour and precipitation in Ivittuut, Southern Greenland, Atmos. Chem. Phys., 14, 4419-2014, https://doi.org/10.5194/acp-14-4419-2014, 2014.

Bonne, J-L., Meyer, H., Behrens, M., Boike, J., Kipfstuhl, S., Rabe, B., Schmidt, T., Schönicke, L., Steen-Larsen, H.C., and Werner, M.: Moisture origin as a driver of temporal variabilities of the water vapour isotopic composition in the Lena River Delta, Siberia, Atmos. Chem. Phys., 20, 10493-10511, https://doi.org/10.5194/acp-20-10493-2020, 2020.

Bookhagen, B., and Burbank, D.W.: Toward a complete Himalayan hydrological budget: Spatiotemporal distribution of snowmelt and rainfall and their impact on river discharge, J. Geophys. Res., 115, F03019, https://doi.org/10.1029/2009JF001426, 2010.

Cai, Z., Tian, L., and Bowen, G.J.: ENSO variability reflected in precipitation oxygen isotopes across the Asian Summer Monsoon region, Earth Planet. Sci. Lett., 475, 25-33, https://doi.org/10.1016/j.epsl.2017.06.035, 2017.

Cai, Z., and Tian, L.: Atmospheric Controls on Seasonal and Interannual Variations in the Precipitation Isotope in the East Asian Monsoon Region, J. Climate, 29, 1339-1352, https://doi.org/10.1175/JCLI-D-15-0363.1, 2016.

Chakraborty, S., Sinha, N., Chattopadhyay, R., Sengupta, S., Mohan, P.M., and Datye, A.: Atmospheric controls on the precipitation isotopes over the Andaman Islands, Bay of Bengal, Sci. Rep., 6, 19555, https://doi.org/10.1038/srep19555, 2016.

Craig, H.: Isotopic Variation in Meteoric Waters. Science, 133, 1702-1703, https://doi.org/10.1126/science.133.3465.1702, 1961.

Craig, H., and Gordon, L.I.: Deuterium and oxygen 18 variation in the ocean and the marine atmosphere, In: Tongiorgi, E. (Eds.), Stable Isotopes in Oceanographic Studies and Paleotemperatures, pp., 9-130, 1965.

Curry, J.A., and Webster, P.J.: Thermodynamics of Atmospheres and Oceans, Academic Press, London, 31705, 1999.

Dai, D., Gao, J., Steen-Larsen, H.C., Yao, T., Ma, Y., Zhu, M., and Li, S.: Continuous monitoring of the isotopic composition of surface water vapor at Lhasa, southern Tibetan Plateau, Atmos. Res., 264, 105827, https://doi.org/10.1016/j.atmosres.2021.105827, 2021.

Dansgaard, W.F.: Stable Isotopes in Precipitation, Tellus B, 16, 436-468, https://doi.org/10.1111/j.2153-3490.1964.tb00181.x, 1964.

Delattre, H., Vallet-Coulomb, C., and Sonzogni, C.: Deuterium excess in the atmospheric water vapour of a Mediterranean coastal wetland: regional vs. local signatures, Atmos. Chem. Phys., 15, 10167-10181, https://doi.org/10.5194/acp-15-10167-2015, 2015.

de Vries, A.J., Aemisegger, F., Pfahl, S., and Wernli, H.: Stable water isotope signals in tropical ice clouds in the West African monsoon simulated with a regional convection-permitting model, Atmos. Chem. Phys., 22, 8863-8895, https://doi.org/10.5194/acp-22-8863-2022, 2022.

Dhar, O., and Rakhecha, P.: Foreshadowing Northeast Monsoon Rainfall Over Tamil Nadu, India, Mon. Weather Rev., 111, 109, https://doi.org/10.1175/1520-0493(1983)111<0109:FNMROT>2.0.CO;2, 1983.

Diekmann, C.J., Schneider, M., Knippertz, P., de Vries, A.J., Pfahl, S., Aemisegger, F., Dahinden, F., Ertl, B., Khosrawi, F., Wernli, H., and Braesicke, P.: A Lagrangian Perspective on Stable Water Isotopes During the West African Monsoon, J. Geophys. Res. Atmos., 126, e2021JD034895, https://doi.org/10.1029/2021JD034895, 2021.

Dirmeyer, P.A., Jin, Y., Singh, B., and Yan, X.: Trends in Land–Atmosphere Interactions from CMIP5 Simulations, J. Hydrometeorol., 14, 829-849, https://doi.org/10.1175/JHM-D-12-0107.1, 2013.

Dütsch, M., Pfahl, S., Meyer, M., and Wernli, H.: Lagrangian process attribution of isotopic variations in near-surface water vapour in a 30-year regional climate simulation over Europe, Atmos. Chem. Phys., 18, 1653-1669, https://doi.org/10.5194/acp-18-1653-2018, 2018.

Gadgil, S.: The Indian Monsoon and Its Variability, Rev. Earth Pl. Sci., 31, 429-467, https://doi.org/10.1146/annurev.earth.31.100901.141251, 2003.

Galewsky, J., and Hurley, J.V.: An advection-condensation model for subtropical water vapor isotopic ratios, J. Geophys. Res. Atmos., 115, 116, https://doi.org/10.1029/2009JD013651, 2010.

Galewsky, J., Steen-Larsen, H.C., Field, R.D., Worden, J., Risi, C., and Schneider, M.: Stable isotopes in atmospheric water vapor and applications to the hydrologic cyclem, Rev. Geophy., 54, 809-865, https://doi.org/10.1002/2015RG000512, 2016.

Gambheer, A.V., and Bhat, G.S.: Life Cycle Characteristics of Deep Cloud Systems over the Indian Region Using INSAT-1B Pixel Data, Mon. Weather Rev., 128, 4071-4083, https://doi.org/10.1175/1520-0493(2000)129<4071:LCCODC>2.0.CO;2, 2000.

Gao, J., Masson-Delmotte, V., Risi, C., He, Y., and Yao, T.: What controls precipitation δ^{18}O in the southern Tibetan Plateau at seasonal and intra-seasonal scales? A case study at Lhasa and Nyalam, Tellus B, 65, 21043, https://doi.org/10.3402/tellusb.v65i0.21043, 2013.

Gao, Y., Li, X., Leung, L. R., Chen, D., and Xu, J.: Aridity changes in the Tibetan Plateau in a warming climate, Environ. Res. Lett., 9, 104013, https://doi.org/10.1088/1748-9326/10/3/034013, 2014.

Gat, J.: Oxygen and hydrogen isotopes in the hydrologic cycle, Annu. Rev. Earth Pl. Sci., 24, 225-262, https://doi.org/10.1146/ANNUREV.EARTH.24.1.225, 1996.

Gedzelman, S., Lawrence, J., Gamache, J., Black, M., Hindman, E., Black, R., Dunion, J., Willoughby, H., and Zhang, X.: Probing hurricanes with stable isotopes of rain and water vapor, Mon. Weather Rev., 131, 1112-1127, https://doi.org/10.1175/1520-0493(2003)131<1112:Phwsio>2.0.Co;2, 2003.

Goff, J.A., and Gratch, S.: Low-pressure properties of water from -160°F to 212 °F. Transactions of the American Society of Heating and Ventilating Engineers, 52, 95-122, 1946.

Goswami, B.N., Venugopal, V., Sengupta, D., Madhusoodanan, M.S., and Xavier, P.K.: Increasing Trend of Extreme Rain Events Over India in a Warming Environment, Science, 314, 1442-1445, https://doi.org/10.1126/science.1132027, 2006.

Graf, P., Wernli, H., Pfahl, S., and Sodemann, H.: A new interpretative framework for below-cloud effects on stable water isotopes in vapour and rain, Atmos. Chem. Phys., 19, 747-765, https://doi.org/10.5194/acp-19-747-2019, 2019.

Guo, X., Tian, L., Wen, R., Yu, W., and Qu, D.: Controls of precipitation $\delta^{18}O$ on the northwestern Tibetan Plateau: A case study at Ngari station, Atmos. Res., 189, 141-151, https://doi.org/10.1016/j.atmosres.2017.02.004, 2017.

Hersbach, H., Bell, B., Berrisford, P., Hirahara, S., Horányi, A., Muñoz Sabater, J., Nicolas, J., Peubey, C., Radu, R., Schepers, D., Simmons, A., Soci, C., Abdalla, S., Abellan, X., Balsamo, G., Bechtold, P., Biavati, G., Bidlot, J., Bonavita, M., and Thépaut, J.N.: The ERA5 global reanalysis, Q. J. Roy. Meteor. Soc., https://doi.org/10.1002/qj.3803, 2020.

Hsu, Y-K., Holsen, T.M., and Hopke, P.K.: Comparison of hybrid receptor models to locate PCB sources in Chicago, Atmos. Environ., 37, 545-562, https://doi.org/10.1016/S1352-2310(02)00886-5, 2003.

Jayasena, H.A.H., Chandrajith, R., and Dissanayake, C.B.: Spatial variation of isotope composition in precipitation in a tropical environment: a case study from the Deduru Oya river basin, Sri Lanka, Hydrol. Process., 22, 4565-4570, https://doi.org/10.1002/hyp.7060, 2008.

Kaushal, N., Breitenbach, S.F.M., Lechleitner, F.A., Sinha, A., Tewari, V.C., Ahmad, S.M., Berkelhammer, M., Band, S., Yadava, M., Ramesh, R., and Henderson, G.M.: The Indian Summer Monsoon from a Speleothem $\delta^{18}O$ Perspective-A Review, Quaternary, 1, 29, https://doi.org/10.3390/quat1030029, 2018.

Kostrova, S.S., Meyer, H., Fernandoy, F., Werner, M., and Tarasov, P.E.: Moisture origin and stable isotope characteristics of precipitation in southeast Siberia, Hydrol. Process., 34, 51-67, https://doi.org/10.1002/hyp.13571, 2020.

Kurita, N.: Origin of Arctic water vapor during the ice-growth season, Geophys. Res. Lett., 38, https://doi.org/10.1029/2010GL046064, 2011.

Kurita, N.: Water isotopic variability in response to mesoscale convective system over the tropical ocean, J. Geophys. Res. Atmos., 118, 10,376-10,390, https://doi.org/10.1002/jgrd.50754, 2013.

Lekshmy, P.R., Midhun, M., and Ramesh, R.: Influence of stratiform clouds on δD and δ^{18}O of monsoon water vapour and rain at two tropical coastal stations, J. Hydrol, 563, 354-362, https://doi.org/10.1016/j.jhydrol.2018.06.001, 2018.

Lekshmy, P.R., Midhun, M., and Ramesh, R.: Role of moisture transport from Western Pacific region on water vapor isotopes over the Bay of Bengal, Atmos. Res., 265, 105895, https://doi.org/10.1016/j.atmosres.2021.105895, 2022.

Lekshmy, P.R., Midhun, M., Ramesh, R., and Jani, R.A.: ^{18}O depletion in monsoon rain relates to large scale organized convection rather than the amount of rainfall, Sci. Rep., 4, 5661, https://doi.org/10.1038/srep05661, 2014.

Li, L., and Garzione, C.N.: Spatial distribution and controlling factors of stable isotopes in meteoric waters on the Tibetan Plateau: Implications for paleoelevation reconstruction, Earth Planet. Sci. Lett., 460, 302-314, https://doi.org/10.1016/j.epsl.2016.11.046, 2017.

Liu, J., Ding, M., and Xiao, C.: Review on atmospheric water vapor isotopic observation and research: theory, method and modeling, Prog. Geog., 34, 340-353, https://doi.org/10.11820/dlkxjz.2015.03.009, 2015.

Liu, X., and Chen, B.: Climatic warming in the Tibetan Plateau during recent decades, Int. J. Climatol., 20, 1729-1742, https://doi.org/10.1002/1097-0088(20001130)20:14<1729::AID-JOC556>3.0.CO;2-Y, 2000.

Majoube, M.: Fractionnement en oxygène 18 entre la glace et la vapeur d'eau, Journal De Chimie Physique, 68, 625-636, 1971a.

Majoube, M.: Fractionnement en oxygène 18 et en deutérium entre l'eau et sa vapeur, Journal de Chimie Physique et de Physico Chimie Biologique, 68, 1423-1436, https://doi.org/10.1051/jcp/1971681423, 1971b.

Malmgren, B.A., Hulugalla, R., Hayashi, Y., and Mikami, T.: Precipitation trends in Sri Lanka since the 1870s and relationships to El Niño-southern oscillation, Int. J. Climatol., 23, 1235-1252, https://doi.org/10.1002/joc.921, 2003.

Masunaga, H., and Kummerow, C.: Observations of tropical precipitating clouds ranging from shallow to deep convective systems, Geophys. Res. Lett., 33, 805, https://doi.org/10.1029/2006GL026547, 2006.

Merlivat, L., and Jouzel, J.: Global climatic interpretation of the deuterium-oxygen 18 relationship for precipitation, J. Geophys. Res. Oceans., 84, 5029-5033. https://doi.org/10.1029/JC084iC08p05029, 1979.

Midhun, M., Lekshmy, P.R., and Ramesh, R.: Hydrogen and oxygen isotopic compositions of water vapor over the Bay of Bengal during monsoon, Geophys. Res. Lett., 40, 6324-6328, https://doi.org/10.1002/2013GL058181, 2013.

Ohring, G., Gruber, A., and Ellingson, R.: Satellite Determinations of the Relationship between Total Longwave Radiation Flux and Infrared Window Radiance, J. Appl. Meteorol. Clim., 23, 416-425, https://doi.org/10.1175/1520-0450(1984)023<0416:SDOTRB>2.0.CO;2, 1984.

Pang, Z., Kong, Y., Froehlich, K., Huang, T., Yuan, L., Li, Z., and Wang, F.: Processes affecting isotopes in precipitation of an arid region, Tellus B, 63, 352-359, https://doi.org/10.1111/j.1600-0889.2011.00532.x, 2011.

Permana, D.S., Thompson, L.G., and Setyadi, G.: Tropical West Pacific moisture dynamics and climate controls on rainfall isotopic ratios in southern Papua, Indonesia, J. Geophys. Res. Atmos., 121, 2222-2245, https://doi.org/10.1002/2015JD023893, 2016.

Pfahl, S., and Wernli, H.: Lagrangian simulations of stable isotopes in water vapor: An evaluation of nonequilibrium fractionation in the Craig-Gordon model, J. Geophys. Res. Atmos., 114, 108, https://doi.org/10.1029/2009JD012054, 2009.

Rahul, P., Ghosh, P., and Bhattacharya, S.K.: Rainouts over the Arabian Sea and Western Ghats during moisture advection and recycling explain the isotopic composition of Bangalore summer rains, J. Geophys. Res. Atmos., 121, 6148-6163, https://doi.org/10.1002/2015JD024579, 2016a.

Rahul, P., Ghosh, P., Bhattacharya, S.K., and Yoshimura, K.: Controlling factors of rainwater and water vapor isotopes at Bangalore, India: Constraints from observations in 2013 Indian monsoon, J. Geophys. Res. Atmos., 121, 13,936-13,952, https://doi.org/10.1002/2016JD025352, 2016b.

Ranjan, S., Al, R., Keesari, T., Singh, V., Kumar, P., and Manish Leuenberger, M.: Triple Water Vapour-Isotopologues Record from Chhota Shigri, Western Himalaya, India: A Unified Interpretation based on δ^{17}O, δ^{18}O, δD and Comparison to Meteorological Parameters, Front. Earth Sci., 8, 599-632, https://doi.org/10.3389/feart.2020.599632, 2021.

Ravisankar, L., Madhavan, M., and Ramesh, R.: Spatial variation of amount effect over peninsular India and Sri Lanka: Role of seasonality, Geophys. Res. Lett., 42, 5500-5507, https://doi.org/10.1002/2015GL064517, 2015.

Risi, C., Bony, S., and Vimeux, F.: Influence of convective processes on the isotopic composition (δ^{18}O and δD) of precipitation and water vapor in the tropics: 2. Physical interpretation of the amount effect, J. Geophys. Res. Atmos., 113, 306, https://doi.org/10.1029/2008JD009943, 2008.

Salamalikis, V., Argiriou, A.A., and Dotsika, E.: Stable isotopic composition of atmospheric water vapor in Patras, Greece: A concentration weighted trajectory approach, Atmos. Res., 152, 93-104, https://doi.org/10.1016/j.atmosres.2014.02.021, 2015.

Saranya, P., Krishan, G., Rao, M.S., Kumar, S., and Kumar, B.: Controls on water vapor isotopes over Roorkee, India: Impact of convective activities and depression systems, J. Hydrol., 557, 679-687, https://doi.org/10.1016/j.jhydrol.2017.12.061, 2018.

Schumacher, C.: Shallow tropical convection: How often does it rain? Bull. Am. Meteorol. Soc., 87, 23-25, 2006.

Singh, P., and Bengtsson, L.: Hydrological sensitivity of a large Himalayan basin to climate change, Hydrol. Process., 18, 2363-2385, https://doi.org/10.1002/hyp.1468, 2004.

Srivastava, R., Ramesh, R., Gandhi, N., Jani, R.A., and Singh, A.K.: Monsoon onset signal in the stable oxygen and hydrogen isotope ratios of monsoon vapor, Atmos. Environ., 108, 117-124, https://doi.org/10.1016/j.atmosenv.2015.02.062, 2015.

Steen-Larsen, H.C., Masson-Delmotte, V., Hirabayashi, M., Winkler, R., Satow, K., Prié, F., Bayou, N., Brun, E., Cuffey, K., Dahl-Jensen, D., Dumont, M., Guillevic, M., Kipfstuhl, J., Landais, A., Popp, T., Risi, C., Steffen, K., Stenni, B., and Sveinbjörnsdottir, A.: What controls the isotopic composition of Greenland surface snow? Clim. Past., 10, 379-392, https://doi.org/10.5194/cpd-9-6035-2013, 2013a.

Steen-Larsen, H.C., Johnsen, S.J., Masson-Delmotte, V., Stenni, B., Risi, C., Sodemann, H., Balslev-Clausen, D., Blunier, T., Dahl-Jensen, D., Ellehøj, M.D., Falourd, S., Grindsted, A., Gkinis, V., Jouzel, J., Popp, T., Sheldon, S., Simonsen, S.B., Sjolte, J., Steffensen, J.P., Sperlich, P., Sveinbjörnsdóttir, A.E., Vinther, B.M., and White, J.W.C.: Continuous monitoring of summer surface water vapor isotopic composition above the Greenland Ice Sheet, Atmos. Chem. Phys., 13, 4815-4828, https://doi.org/10.5194/acp-13-4815-2013, 2013b.

Steen-Larsen, H.C., Sveinbjörnsdottir, A.E., Jonsson, T., Ritter, F., Bonne, J-L., Masson-Delmotte, V., Sodemann, H., Blunier, T., Dahl-Jensen, D., and Vinther, B.M.: Moisture sources and synoptic to seasonal variability of North Atlantic water vapor isotopic composition, J. Geophys. Res. Atmos., 120, 5757-5774, https://doi.org/10.1002/2015JD023234, 2015.

Stewart, M.K.: Stable isotope fractionation due to evaporation and isotopic exchange of falling waterdrops: Applications to atmospheric processes and evaporation of lakes, J. Geophys. Res., 80, 1133-1146, https://doi.org/10.1029/JC080i009p01133, 1975.

Sturm, P., and Knohl, A.: Water vapor δ^2H and δ^{18}O measurements using off-axis integrated cavity output spectroscopy, Atmos. Meas. Tech., 3, 67-77, https://doi.org/10.5194/amt-3-67-2010, 2010.

Thompson, L.G., Davis, M.E., Mosley-Thompson, E., Beaudon, E., Porter, S.E., Kutuzov, S., Lin, P.N., Mikhalenko, V.N., and Mountain, K.R.: Impacts of Recent Warming and the 2015/2016 El Niño on Tropical Peruvian Ice Fields, J. Geophys. Res. Atmos., 122, 12,688-12,701, https://doi.org/10.1002/2017JD026592, 2017.

Tremoy, G., Vimeux, F., Mayaki, S., Souley, I., Cattani, O., Risi, C., Favreau, G., and Oi, M.: A 1-year long δ^{18}O record of water vapor in Niamey (Niger) reveals insightful atmospheric processes at different timescales, Geophys. Res. Lett., 39(8), 805, https://doi.org/10.1029/2012GL051298, 2012.

Uemura, R., Matsui, Y., Yoshimura, K., Motoyam, H., and Yoshida, N.: Evidence of deuterium excess in water vapor as an indicator of ocean surface conditions, J. Geophys. Res. Atmos., 113, D19114, https://doi.org/10.1029/2008JD010209, 2008.

Villiger, L., and Aemisegger, F.: Water isotopic characterisation of the cloud–circulation coupling in the North Atlantic trades – Part 2: The imprint of the atmospheric circulation at different scales, Atmos. Chem. Phys., 24, 957-976, https://doi.org/10.5194/acp-24-957-2024, 2024.

Vimeux, F., Tremoy, G., Risi, C., and Gallaire, R.: A strong control of the South American SeeSaw on the intra-seasonal variability of the isotopic composition of precipitation in the Bolivian Andes, Earth. Planet. Sci. Lett., 307, 47-58, https://doi.org/10.1016/j.epsl.2011.04.031, 2011.

Wallace, J.M., and Hobbs, P.V.: 3-Atmospheric Thermodynamics, Atmos. Sci., 63-111, https://doi.org/10.1016/B978-0-12-732951-2.50008-9, 2006.

Wang, B.: The Asian monsoon. Springer praxis books, Springer/Praxis Publishing Co, Berlin, 787 pp., 651-683, 2006.

Webster, P.J., Magana, V.O., Palmer, T.N., Shukla, J., Tomas, R.A., Yanai, M., and Yasunari, T.: Monsoons: Processes, predictability, and the prospects for prediction, J. Geophys. Res. Oceans., 103, 14451-14510, https://doi.org/10.1029/97JC02719, 1998.

Worden, J., Noone, D., Bowman, K., Beer, R., Eldering, A., Fisher, B., Gunson, M., Goldman, A., Herman, R., Kulawik, S., Lampel, M., Osterman, G., Rinsland, C., Rodgers, C., Sander, S., Shephard, M., Webster, C., and Worden, H.: Importance of rain evaporation and continental convection in the tropical water cycle, Nature, 445, 528-532, https://doi.org/10.1038/nature05508, 2007. Xu, T., Pang, H., Zhan, Z., Zhang, W., Guo, H., Wu, S., and Hou, S.: Water vapor isotopes indicating rapid shift among multiple moisture sources for the 2018-2019 winter extreme precipitation events in southeastern China, Hydrol. Earth Syst. Sci., 26, 117-127, https://doi.org/10.5194/hess-26-117-2022, 2022.

Yao, T., Thompson, L.G., Mosbrugger, V., Zhang, F., Ma, Y., Luo, T., Xu, B., Yang, X., Joswiak, D.R., Wang, W., Joswiak, M.E., Devkota, L.P., Tayal, S., Jilani, R., and Chen, F.: Third Pole Environment (TPE), Environ. Dev., 7, 52-64, https://doi.org/10.1016/j.envdev.2012.04.002, 2012.